Scientia Iranica F (2013) 20(6), 2356–2374

SCIENTIA IRANICA

Sharif University of Technology
Scientia Iranica
Transaction F: Nanotechnology
www.scientiairanica.com

Surface stress effects on dynamic stability of double-walled boron nitride nanotubes conveying viscose fluid based on nonlocal shell theory

A. Ghorbanpour Arani[a,b,*] and M. Hashemian[a]

a. *Faculty of Mechanical Engineering, University of Kashan, Kashan, Iran.*
b. *Institute of Nanoscience and Nanotechnology, University of Kashan, Kashan, Iran.*

Received 13 January 2013; received in revised form 3 June 2013; accepted 22 July 2013

KEYWORDS
DWBNNT;
Dynamic stability;
Surface stress effects;
Piezoelasticity;
Viscose fluid.

Abstract. In the present study, the dynamic stability of double-walled boron nitride nanotubes (DWBNNTs) including surface stress effects, is investigated, based on the Gurtin-Murdoch continuum theory. Nonlocal piezoelasticity is incorporated into shell theory to develop a non-classical model for DWBNNT. The effects of van der Waals (vdW) forces, viscose fluid passes through the inner nanotube and visco-Pasternak medium are evaluated. Fluid-DWBNNT interaction is evaluated considering the slip boundary condition and bulk viscosity. Hamilton's principle is utilized to derive governing equations with regard to von Kármán geometric nonlinearity. Finally, the Incremental Harmonic Balance Method (IHBM) indicates the Dynamic Instability Region (DIR) of DWBNNT. A detailed parametric study is conducted, focusing on the combined effects of the surface parameters, nonlocality, fluid velocity, Knudsen number, thermal changes, vdW forces and surrounding medium on the DIR of DWBNNT. Numerical results indicate that considering surface stress effects shifts the DIR to a higher frequency zone.

1. Introduction

Carbon nanotubes (CNTs) and boron nitride nanotubes (BNNTs) have a similar hexagonal structure and both are produced by rolling corresponding sheets. BNNTs have more resistance to oxidation at high temperature than other conventional nanotubes such as CNTs, so they can be used in equipment with high thermal resistance. CNTs exhibit metallic or semiconducting properties depending on their chirality, but BNNTs are always considered semi-conducting materials which are approximately independent of chirality. Unlike CNTs, BNNTs have a strong piezoelectric property. This property makes them a novel choice for producing sensors, actuators and other smart control applications, such as the reinforcement of smart nanocomposites. BNNTs possess extraordinary properties, such as high elastic modulus, high thermal conductivity, low density, constant wide band gap, superb structural stability and chemical inertness. BNNTs, in general, have two highly symmetrical structures: zigzag and armchair. For uniaxial strain, zigzag tubes exhibit a longitudinal piezoelectric response, while the armchair tubes have an electric dipole moment linearly coupled to torsion [1].

Fluid-conveying structures have attracted a large number of studies in literature [2-5]. In recent years, a large amount of research work has been carried out on the buckling and vibration of nanotubes with conveying fluid due to the application of nanotubes as fluid transport, gas storage and drug delivery devices. In

*. *Corresponding author. Tel.: +98 3615912450; Fax: +98 3615912424*
E-mail address: aghorban@kashanu.ac.ir (A. Ghorbanpour Arani)

order to mechanically model these structures, higher-order continuum theories, such as partial nonlocal elasticity, exact nonlocal elasticity, nonlocal piezoelasticity, modified couple stress, strain gradient elasticity and surface elasticity theory have been recently employed. Khosravian and Rafii-Tabar [6] investigated viscous fluid through Multi-Walled CNTs (MWCNTs) for the first time. The dynamic behavior of triple-walled CNTs is reported by Yan et al. [7] considering the vdW effect. Lee and Chang [8] reported the linear vibration of Double-Walled CNTs (DWCNTs) conveying fluid based on nonlocal continuum mechanics. The effect of internal moving fluid and compressive load on the nonlinear vibration and stability of CNTs is reported by Rasekh and Khadem [9] based on the method of multiple scales. Results show that beyond critical fluid velocity, buckling occurs. Wang and Ni [10] showed that the effect of viscosity can be ignored in the vibration analysis of CNTs conveying viscous fluid. Wang [11] found that the effect of small length parameters on critical flow velocity can be ignored in the vibration analysis of DWCNTs. Noncoaxial vibration of fluid-filled MWCNTs is studied by Yan et al. [12]. Ghavanloo et al. [13] studied the effect of viscoelastic Winkler foundation on the instability of CNTs conveying fluid. They also obtained the effect of viscoelastic modulus and damping factors on the resonance frequency of the CNTs, based on the Finite Element Method (FEM). The vibration and instability of DWCNTs, based on the modified couple stress theory, which contains a material length parameter, are investigated by Ke and Wang [14]. Results show that the imaginary component of the frequency and critical fluid velocity of the fluid-conveying DWCNTs increase with an increase in the length scale parameter. Farshidianfar and Soltani [15] investigated the nonlinear flow-induced vibration of Single-Walled CNTs (SWCNTs) considering geometrical imperfection based on the nonlocal continuum theory. The surrounding medium is assumed as a Pasternak type and the effect of imperfection on nonlinear frequency is discussed using the method of multiple scales. Rashidi et al. [16] reported a novel model for the vibration of nanotubes conveying nanoflow. The effect of small-size on the bulk viscosity and slip boundary conditions of nanoflow through Knudsen number (K_n) is considered in this paper. They found that incorporating the nanoflow slip boundary conditions hypothesis changes the results drastically, as compared to continuum flow models. Khoddami Maraghi et al. [17] studied the vibration and instability of DWBNNT conveying viscous fluid using the nonlocal piezoelasticity theory and the Differential Quadrature Method (DQM). The nonlinear dynamic response of embedded fluid-conveyed micro-tube reinforced by BNNTs is investigated by Ghorbanpour Arani et al. [18]. Results show that electric and thermal loadings are the controlling parameters to improve the stability of the smart composite micro-tube. Ghorbanpour Arani et al. [19] reported the nonlinear nonlocal vibration of embedded DWCNT conveying fluid using a shell model. According to this study, increasing the circumferential wave number leads to enhanced nonlinearity. Nonlocal wave propagation in an embedded DWBNNT conveying fluid via the strain gradient theory is reported by Ghorbanpour Arani et al. [20]. They found that the phase velocities predicted by the strain gradient theory are lower than those predicted by Eringen's theory, because strain gradient and Eringen theories contain three and one material length scale parameters to capture the size effect, respectively.

The partial nonlocal elasticity theory derives a higher-order equation of motion without the corresponding higher-order boundary conditions, but the exact nonlocal elasticity theory derives a higher-order governing differential equation with the corresponding higher-order boundary conditions via the variational principle. Recently, Lim [21] successfully established an exact nonlocal elasticity theory and proved that the stiffness of a nanobeam is strengthened with the presence of a nonlocal nanoscale.

As discussed above, the dynamic stability of nanotubes conveying fluid is not reported in literature. Few studies have been done on the dynamic response of CNTs. Ansari et al. [22] reported the dynamic stability of SWCNT, including thermal environment effects, based on Timoshenko beam and Euler-Bernoulli beam theories. Results of linear dynamic stability show that the difference between the instability region of local and nonlocal beams is significant for nanotubes with lower aspect ratios. Nonlinear dynamic instability of DWCNT under periodic excitation is reported by Fu et al. [23], based on Euler-Bernoulli beam theory. Results show that the area of DIR could be reduced by a stiffness medium and an increment in the aspect ratio of nanotubes. Recently, Li and Wang [24] reported the effect of small scale on the dynamic characteristic of CNTs under axially oscillating loading. Parametric resonance frequency is observed in the range of oscillating frequencies, even for dynamic oscillating loads smaller than the static buckling load.

Due to differences between the bulk and surface properties, Gurtin and Murdoch developed classical continuum mechanics [25]. The surface layer surrounds the material bulk without slipping. In nano structures, due to the high surface area to volume ratio, the effect of the surface is significant [26,27]. The vibration analysis of fluid-conveying nanotubes considering surface effects is investigated by Wang [28]. The results show that the surface effects with positive elastic constant or positive tensile residual surface stress tend to increase the natural frequency and

critical flow velocity. Wang [29] studied the nonlinear buckling analysis of nanobeams containing internal flowing fluid. According to this study, the effect of surface on buckling amplitude is very strong. Lei et al. [30] investigated surface effects on the vibration analysis of DWCNT based on the Timoshenko beam theory.

As illustrated above, the dynamic stability of BNNT is not reported in literature. In this article, the dynamic stability of DWBNNTs is studied considering internal viscose flowing fluid. Axial oscillating loading is applied to the DWBNNT in a thermal environment. Higher order nonlocal shell theory is used to derive the nonlinear governing equations of embedded DWBNNT considering electric-mechanical coupling. Also, the effects of surface stress, nonlinear vdW forces and visco-Pasternak medium are studied in this survey. Galerkin and IHBMs are used to discretize space and time domains and, finally, an iterative approach indicates the DIR of DWBNNT.

2. Deriving governing equations

Figure 1 shows a DWBNNT conveying flowing fluid in a visco-Pasternak medium. This figure shows a DWBNNT with inner radius, R_1, outer radius, R_2, thickness, h, and length, L. The fluid velocity through the DWBNNT is assumed as V_0 in this study.

2.1. Nonlinear shell model

DWBNNT is modeled as coaxial cylindrical shells. According to Donnell's cylindrical shell theory, the displacement field can be expressed as:

$$\tilde{u}_i(x,\theta,z,t) = u_i(x,\theta,t) - z\frac{\partial w_i(x,\theta,t)}{\partial x},$$

$$\tilde{v}_i(x,\theta,z,t) = v_i(x,\theta,t) - \frac{z}{R_i}\frac{\partial w_i(x,\theta,t)}{\partial \theta},$$

$$\tilde{w}_i(x,\theta,z,t) = w_i(x,\theta,t), \tag{1}$$

where $\tilde{u}_i$, $\tilde{v}_i$ and $\tilde{w}_i$ are the total displacements in the axial (x), circumferential (θ) and radial (z) directions of the inner ($i = 1$) and outer ($i = 2$) tubes; u_i, v_i and w_i are the corresponding middle surface displacements; and t represents time. The strain-displacement relationship, according to the von Kármán nonlinear theory, can be expressed as:

$$\varepsilon_{xi} = u_{i,x} + \frac{1}{2}{w_{i,x}}^2 - z w_{i,xx},$$

$$\varepsilon_{\theta i} = \frac{1}{R_i}(v_{i,\theta} + w_i) + \frac{1}{2R_i^2}{w_{i,\theta}}^2 - \frac{z}{R_i^2} w_{i,\theta\theta},$$

$$\gamma_{x\theta i} = \frac{1}{R_i} u_{i,\theta} + v_{i,x} + \frac{1}{R_i} w_{i,x} w_{i,\theta} - \frac{2z}{R_i} w_{i,x\theta}. \tag{2}$$

2.2. Fluid-DWBNNT interaction

The velocity components of the flowing fluid in the axial, radial and circumferential directions can be expressed as [3]:

$$V_x = \frac{\partial \tilde{u}_1}{\partial t} + V_0\cos(\varsigma),$$

$$V_r = \frac{\partial \tilde{w}_1}{\partial t} + V_0\sin(\varsigma),$$

$$V_\theta = \frac{\partial \tilde{v}_1}{\partial t}, \tag{3}$$

where ς represents the attack angle of flow. The above equations can be simplified by considering $\cos(\varsigma) = 1$ and $\sin(\varsigma) = \frac{\partial w_1}{\partial x}$ [3]. To evaluate the interaction

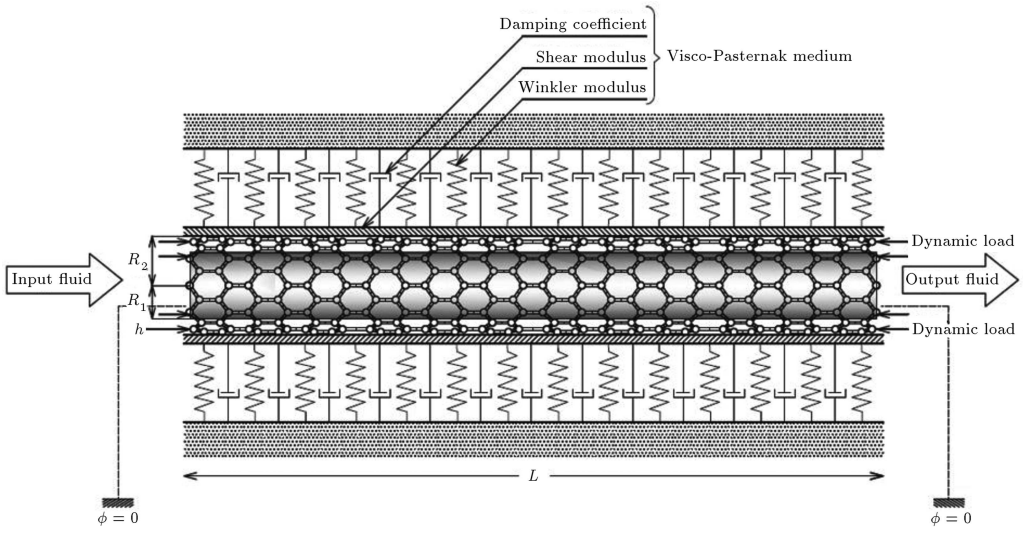

Figure 1. DWBNNT conveying fluid embedded in visco-Pasternak medium.

between DWBNNT and fluid, considering the viscosity effect, Navier-Stokes equation can be used, as:

$$\rho_f \frac{DV}{Dt} = -\nabla p + \rho_f g + \mu \nabla^2 V, \tag{4}$$

where μ, ρ_f and p are the viscosity, density and pressure of the fluid, respectively, and $\frac{D}{Dt}$ represents the material derivative. The energy of viscosity terms can be calculated applying an integral on the fluid area (A_f) to derive governing equations ($V_f = \iint p_{,r} w_1 dx dA_f$) [17]. As described in [16], a modified Navier-stokes equation should be used to consider the small-size effects on the flow field. However, the viscosity of the fluid should be replaced with effective viscosity (μ_e) in Eq. (4), which is a function of Knudsen number (K_n) as follows:

$$\mu_e = \mu_0 \left(\frac{1}{1 + aK_n} \right), \tag{5}$$

where μ_0 is the bulk viscosity and a is a coefficient [16]. Eq. (4) should be modified to consider slip boundary conditions. Hence, the Velocity Correction Factor (VCF) is calculated as [16]:

$$\begin{aligned} \text{VCF} &= \frac{V_{\text{avg,slip}}}{V_{\text{avg,no slip}}} \\ &= (1 + aK_n) \left(4 \left(\frac{2 - \sigma_v}{\sigma_v} \right) \left(\frac{K_n}{1 + K_n} \right) + 1 \right), \end{aligned} \tag{6}$$

where $V_{\text{avg,slip}}$ and $V_{\text{avg,no slip}}$ are average flow velocities through the nanotube, considering the slip boundary condition and ignoring it. Also, σ_v is dependent on the molecules tangential momentum [16]. The average flow velocity of no-slip boundary conditions could be used instead of the average flow velocity of slip-boundary conditions by applying a velocity correction factor.

2.3. Energy method

Governing dynamic equations of DWBNNT are derived using an energy method. Different energy components are calculated in this section. Strain energy can be expressed as:

$$\Pi_i = \frac{1}{2} \iiint \left(\sigma_{xi} \varepsilon_{xi} + \sigma_{\theta i} \varepsilon_{\theta i} + \sigma_{x\theta i} \gamma_{x\theta i} \right) R_i dx d\theta dz. \tag{7}$$

The kinetic energy of the DWBNNT can be evaluated as:

$$K_i = \frac{1}{2} \iiint \rho_t \left(\dot{\tilde{u}}_i^2 + \dot{\tilde{v}}_i + \dot{\tilde{w}}_i \right) R_i dx d\theta dz, \tag{8}$$

where ρ_t denotes the mass density of BNNT and the dot indicates the time derivation. Also, the kinetic energy of fluid passing through the inner BNNT is:

$$\begin{aligned} K_f =& \frac{1}{2} \iint \rho_f \Big[\left(\dot{\tilde{u}}_1 + V_{\text{avg,slip}} \right)^2 \\ &+ \left(\dot{\tilde{w}}_1 + V_{\text{avg,slip}} w_{1,x} \right)^2 + \dot{\tilde{v}}_1^2 \Big] dx dA_f. \end{aligned} \tag{9}$$

The Lennard-Jones model is used to evaluate the vdW interlayer force in DWBNNT, so the work done regarding the visco-Pasternak medium and vdW effect can be expressed as:

$$V_v = \frac{1}{2} \int_0^L q_1 w_1 dx + \frac{1}{2} \int_0^L q_2 w_2 dx + \frac{1}{2} \int_0^L -F_m w_2 dx, \tag{10}$$

where q_1 and q_2 represent the interlayer vdW interaction and F_m is the visco-Pasternak effect:

$$\begin{aligned} q_1 &= c(w_2 - w_1) + c_n (w_2 - w_1)^3, \\ q_2 &= -c(w_2 - w_1) - c_n (w_2 - w_1)^3, \\ F_m &= K_w w_2 + cv \dot{w}_2 - K_G w_{2,xx}, \end{aligned} \tag{11}$$

where c and c_n are the linear and nonlinear vdW coefficients, K_w and K_G are the spring and shear constants of the Winkler and Pasternak foundations and cv is the damping factor of the visco medium. The electric field energy is:

$$V_{ei} = \int D_{xi} E_{xi} dV, \tag{12}$$

where D_{xi} and E_{xi} are the electric displacement and electric field in the axial direction for the ith tube, respectively. The relation between the electric field and the electric potential (φ_x) is expressed as:

$$E_{xi} = -\frac{\partial \varphi_{xi}}{\partial x}. \tag{13}$$

2.4. Hamilton's principle

The governing equations can be derived using Hamilton's principle:

$$\begin{aligned} \delta \int_0^t (\Pi_1 + \Pi_2 - K_1 - K_2 - K_f - V_v \\ - V_{e1} - V_{e2} - \delta V_f) dt = 0. \end{aligned} \tag{14}$$

Substituting the energy terms into Eq. (14) and setting the coefficients of δu_i, δw_i, δv_i and $\delta \varphi_{xi}$ to zero results

in:

δu_i :

$$-N_{xi,x}-\frac{1}{R_i}N_{x\theta i,\theta}+\rho_t h\ddot{u}_i+m_0\frac{1}{2R_1}\rho_f R_{1I}^2\ddot{u}_1=0, \tag{15a}$$

δw_i :

$$\begin{aligned}&-\left[N_{xi}w_{i,x}\right]_{,x}-M_{xi,xx}+\frac{N_{\theta i}}{R_i}-\frac{1}{R_i^2}\left[N_{\theta i}w_{i,\theta}\right]_{,\theta}\\&-\frac{1}{R_i^2}M_{\theta i,\theta\theta}-\frac{2}{R_i}N_{x\theta i}w_{i,x\theta}\\&-\frac{1}{R_i}N_{x\theta i,\theta}w_{i,x}-\frac{1}{R_i}N_{x\theta i,x}w_{i,\theta}\\&-\frac{2}{R_i}M_{x\theta i,x\theta}-\frac{\rho_t h^3}{12}\ddot{w}_{i,xx}-\frac{\rho_t h^3}{12}\frac{1}{R_i^2}\ddot{w}_{i,\theta\theta}\\&+\rho_t h\ddot{w}_i+\rho_f m_0\left[\frac{R_{1I}^2}{2R_1}\ddot{w}_1\right.\\&+\rho_f\frac{R_{1I}^2}{2R_1}\left(\mathrm{VCFV}_{\text{avg,no slip}}\right)^2 w_{1,xx}\\&+\rho_f\frac{R_{1I}^2}{R_1}\mathrm{VCFV}_{\text{avg,no slip}}\dot{w}_{1,x}\\&\left.-\rho_f\frac{R_{1I}^4}{8R_1}\left(\ddot{w}_{1,xx}+\frac{1}{R_1^2}\ddot{w}_{1,\theta\theta}\right)\right]\\&=\mu_e\frac{R_{1I}^2}{2R_1}m_0\left[\dot{w}_{1,xx}+\mathrm{VCFV}_{\text{avg,no slip}}w_{1,xxx}\right.\\&+\frac{1}{R_{1I}^2}\dot{w}_{1,\theta\theta}-\frac{1}{R_{1I}^2}\dot{w}_1\\&+\mathrm{VCFV}_{\text{avg,no slip}}\frac{1}{R_{1I}^2}w_{1,x\theta\theta}\\&\left.-\frac{1}{R_{1I}^2}\mathrm{VCFV}_{\text{avg,no slip}}w_{1,x}-\frac{2}{R_{1I}^2}\dot{v}_{1,\theta}\right]\\&-(-1)^i\frac{R_{1o}}{R_i}(c(w_2-w_1)+c_n(w_2-w_1)^3)\\&-m_1\frac{R_{2o}}{R_i}(K_w w_2+cv\dot{w}_2-K_G\nabla^2 w_2),\end{aligned} \tag{15b}$$

δv_i :

$$-\frac{1}{R_i}N_{\theta i,\theta}-N_{x\theta i,x}+\rho_t h\ddot{v}_i+m_0\rho_f\frac{R_{1I}^2}{2R_1}\ddot{v}_1=0, \tag{15c}$$

$\delta\varphi_{xi}$:

$$D_{xi,x}=0, \tag{15d}$$

where R_{iI} and R_{io} are the internal and external radius of the ith tube, and N_{xi} and M_{xi} are the resultant force and moment per unit length, which are defined as:

$$\begin{aligned}&N_{xi}=\int\sigma_{xi}dz, \qquad N_{\theta i}=\int\sigma_{\theta i}dz,\\&N_{x\theta i}=\int\sigma_{x\theta i}dz, \qquad M_{xi}=\int\sigma_{xi}zdz,\end{aligned} \tag{16}$$

and $m_0=0$ for $i=2$ and $m_0=1$ for $i=1$. Also $m_1=0$ for $i=1$ and $m_1=1$ for $i=2$.

Neglecting the effects of flowing fluid, nonlinear vdW force and the damping factor of the medium, Eqs. (15) reduce to the governing equations of Ref. [31].

3. Surface elasticity theory

According to the Gurtin-Murdoch theory, the interaction between the surface and bulk material causes in-plane loads on BNNT [32] as:

$$\begin{aligned}&\sigma_{xi}^s=(2\mu_s+\lambda_s)\varepsilon_{xi}+2\tau^s,\\&\sigma_{\theta i}^s=(2\mu_s+\lambda_s)\varepsilon_{\theta i}+2\tau^s,\\&\sigma_{xzi}^s=\tau^s w_{i,x},\\&\sigma_{\theta zi}^s=\frac{1}{R_i}\tau^s w_{i,\theta},\end{aligned} \tag{17}$$

where μ_s and λ_s are the surface Lame constants and τ^s is the residual surface stress under an unstrained condition; all of them having the (N/m) unit. Also, superscript s refers to the surface layer. In Eq. (17), σ can be replaced by N, according to Eq. (16). Unlike classical beam theory, stress in a radial direction is significant, considering the surface stress effect, and changes linearly through the surface thickness [25,32,33] (see Eq. (18) in Box I).

4. Nonlocal piezoelasticity theory

Nonlocal constitutive relations for a Donnell cylindrical shell considering surface effect can be expressed as [19,31,32,34]:

$$\begin{aligned}N_{xi}-(e_0a)^2\nabla^2N_{xi}=&\frac{Eh}{1-\upsilon^2}\left(u_{i,x}+\frac{1}{2}w_{i,x}^2\right.\\&\left.+\frac{\upsilon}{R_i}\left(v_{i,\theta}+w_i\right)+\frac{\upsilon}{2R_i^2}w_{i,\theta}^2\right)\\&-\frac{EhT(\alpha_x+\upsilon\alpha_\theta)}{1-\upsilon^2}-h_{11}E_{xi}h,\end{aligned} \tag{19a}$$

$$\sigma_z = \frac{\left(\sigma^s_{xz,x} + \frac{1}{R}\sigma^s_{\theta z,\theta} - \rho^s\ddot{w}\right)_{\text{at top}} + \left(\sigma^s_{xz,x} + \frac{1}{R}\sigma^s_{\theta z,\theta} - \rho^s\ddot{w}\right)_{\text{at bottom}}}{2} - \frac{\left(\sigma^s_{xz,x} + \frac{1}{R}\sigma^s_{\theta z,\theta} - \rho^s\ddot{w}\right)_{\text{at top}} - \left(\sigma^s_{xz,x} + \frac{1}{R}\sigma^s_{\theta z,\theta} - \rho^s\ddot{w}\right)_{\text{at bottom}}}{h} z. \quad (18)$$

Box I

$$N_{\theta i} - (e_0a)^2\nabla^2 N_{\theta i} = \frac{Eh}{1-\upsilon^2}\left(\frac{1}{R_i}v_{i,\theta} + \frac{w_i}{R_i} + \frac{1}{2R_i^2}{w_{i,\theta}}^2 + \upsilon u_{i,x} + \frac{\upsilon}{2}w_{i,x}^2\right) - \frac{EhT\left(\alpha_\theta + \upsilon\alpha_x\right)}{1-\upsilon^2}, \quad (19b)$$

$$N_{x\theta i} - (e_0a)^2\nabla^2 N_{x\theta i} = \frac{Eh}{2(1+\upsilon)}\left(\frac{1}{R_i}u_{i,\theta} + v_{i,x} + \frac{1}{R_i}w_{i,\theta}w_{i,x}\right), \quad (19c)$$

$$M_{xi} - (e_0a)^2\nabla^2 M_{xi} = \frac{-Eh^3}{12(1-\upsilon^2)}\left(w_{i,xx} + \frac{\upsilon}{R_i^2}w_{i,\theta\theta}\right) + \frac{\upsilon h^2}{6(1-\upsilon)}\left(\tau^s w_{i,xx} + \tau^s\frac{1}{R_i^2}w_{i,\theta\theta} - \rho^s\ddot{w}_i\right), \quad (19d)$$

$$M_{\theta i} - (e_0a)^2\nabla^2 M_{\theta i} = \frac{-Eh^3}{12(1-\upsilon^2)}\left(\frac{1}{R_i^2}w_{i,\theta\theta} + \upsilon w_{i,xx}\right) + \frac{\upsilon h^2}{6(1-\upsilon)}\left(\tau^s w_{i,xx} + \tau^s\frac{1}{R_i^2}w_{i,\theta\theta} - \rho^s\ddot{w}_i\right), \quad (19e)$$

$$M_{x\theta i} - (e_0a)^2\nabla^2 M_{x\theta i} = \frac{-Eh^3}{12(1+\upsilon)}\left(\frac{1}{R_i}w_{i,x\theta}\right), \quad (19f)$$

$$D_{xi} - (e_0a)^2\nabla^2 D_{xi} = h_{11}\left(\frac{\partial u_i}{\partial x} + \frac{1}{2}\left(\frac{\partial w_i}{\partial x}\right)^2 + z\frac{\partial\psi_i}{\partial x} - \alpha_x T\right) + \zeta_{11}E_{xi}, \quad (19g)$$

where e_0a, E, T, h_{11}, ζ_{11}, α_x and α_θ represent the nonlocal parameter, Young's modulus, thermal changes, piezoelectric coefficient, dielectric permittivity, and thermal expansion coefficients in axial and circumferential directions, respectively. Also (∇^2) denotes the Laplace operator [31]. The above equations can be applied to bulk material. Considering Eq. (17), nonlocal equations for the surface layer in electric and thermal environments can be derived as:

$$(1-(e_0a)^2\nabla^2)N^s_{xi} = (2\mu_s+\lambda_s)(\varepsilon_{xi} - \alpha^s_x T) - h^s_{11}E_{xi} + 2\tau^s, \quad (20a)$$

$$(1-(e_0a)^2\nabla^2)N^s_{\theta i} = (2\mu_s+\lambda_s)(\varepsilon_{\theta i} - \alpha^s_x T) + 2\tau^s, \quad (20b)$$

$$(1-(e_0a)^2\nabla^2)M^s_{xi} = -(2\mu_s+\lambda_s)\left(\frac{R_{iI}^2 + R_{io}^2}{2}w_{i,xx}\right), \quad (20c)$$

$$(1-(e_0a)^2\nabla^2)M^s_{\theta i} = -(2\mu_s+\lambda_s)\left(\frac{R_{iI}^2 + R_{io}^2}{2R_i^2}w_{i,\theta\theta}\right), \quad (20d)$$

$$(1-(e_0a)^2\nabla^2)D^s_{xi} = h^s_{11}\left(u_{i,x} + \frac{1}{2}{w_{i,x}}^2 - \alpha^s_x T\right) + \zeta^s_{11}E_{xi}, \quad (20e)$$

The final governing equations are derived by substituting Eqs. (19)-(20) into Eq. (15) as:

$$\left[\frac{Eh}{1-\upsilon^2}\left(u_{i,x} + \frac{1}{2}{w_{i,x}}^2 + \frac{\upsilon}{R_i}(v_{i,\theta} + w_i) + \frac{\upsilon}{2R_i^2}w_{i,\theta}^2\right) - \frac{EhT(\alpha_x + \upsilon\alpha_\theta)}{1-\upsilon^2} - h_{11}E_{xi}h\right]_{,x} + \left[(2\mu_s+\lambda_s)\left(u_{i,x} + \frac{1}{2}w_{i,x}^2 - \alpha^s_x T\right)\right.$$

$$
\begin{aligned}
&- h_{11}^{s}E_{xi} + 2\tau^{s}\Big]_{,x} + \frac{1}{R_i}\left[\frac{Eh}{2(1+\upsilon)}\left(\frac{1}{R_i}u_{i,\theta}\right.\right.\\
&\left.\left.+ v_{i,x} + \frac{1}{R_i}w_{i,\theta}w_{i,x}\right)\right]_{,\theta}\\
&= (1-(e_0a)^2\nabla^2)\left[(\rho_t h + 2\rho^s)\ddot{u}_i\right.\\
&\left.+ m_0\frac{1}{2R_1}\rho_f R_{1I}^2\ddot{u}_1\right], \qquad (21a)\\
&-(1-(e_0a)^2\nabla^2)\left\{[N_{xi}w_{i,x}]_{,x} + \frac{1}{R_i^2}[N_{\theta i}w_{i,\theta}]_{,\theta}\right.\\
&\left.+ \frac{2}{R_i}N_{x\theta i}w_{i,x\theta} + \frac{1}{R_i}N_{x\theta i,\theta}w_{i,x} + \frac{1}{R_i}N_{x\theta i,x}w_{i,\theta}\right\}\\
&- \left[\frac{-Eh^3}{12(1-\upsilon^2)}\left(w_{i,xx} + \frac{\upsilon}{R_i^2}w_{i,\theta\theta}\right)\right.\\
&\left.+ \frac{\upsilon h^2}{6(1-\upsilon)}\left(\tau^s w_{i,xx} + \frac{\tau^s}{R_i^2}w_{i,\theta\theta} - \rho^s\ddot{w}_i\right)\right]_{,xx}\\
&+ \left[(2\mu_s+\lambda_s)\left(\frac{R_{iI}^2+R_{io}^2}{2}w_{i,xx}\right)\right]_{,xx} - 2\tau^s w_{i,xx}\\
&+ \frac{1}{R_i}\left[\frac{Eh}{1-\upsilon^2}\left(\frac{1}{R_i}v_{i,\theta} + \frac{w_i}{R_i} + \frac{1}{2R_i^2}{w_{i,\theta}}^2\right.\right.\\
&\left.\left.+ \upsilon u_{i,x} + \frac{\upsilon}{2}w_{i,x}^2\right) - \frac{EhT(\alpha_\theta+\upsilon\alpha_x)}{1-\upsilon^2}\right]\\
&+ \frac{1}{R_i}\left[(2\mu_s+\lambda_s)\left(\frac{1}{R_i}(v_{i,\theta}+w_i) + \frac{1}{2R_i^2}{w_{i,\theta}}^2\right.\right.\\
&\left.\left.- \alpha_\theta^s T\right) + 2\tau^s\right] - \frac{1}{R_i^2}\left[\frac{-Eh^3}{12(1-\upsilon^2)}\left(\frac{1}{R_i^2}w_{i,\theta\theta}\right.\right.\\
&\left.\left.+ \upsilon w_{i,xx}\right) + \frac{\upsilon h^2}{6(1-\upsilon)}\left(\tau^s w_{i,xx} + \frac{\tau^s}{R_i^2}w_{i,\theta\theta}\right.\right.\\
&\left.\left.-\rho^s\ddot{w}_i\right)\right]_{,\theta\theta} + \frac{1}{R_i^2}\left[(2\mu_s+\lambda_s)\left(\frac{R_{iI}^2+R_{io}^2}{2R_i^2}w_{i,\theta\theta}\right)\right]_{,\theta\theta}\\
&- 2\tau^s\frac{1}{R_i^2}w_{i,\theta\theta} + \frac{2}{R_i}\left[\frac{Eh^3}{12(1+\upsilon)}\left(\frac{1}{R_i}w_{i,x\theta}\right)\right]_{,x\theta}\\
&= (1-(e_0a)^2\nabla^2)\left[\mu_e\frac{R_{1I}^2}{2R_1}m_0\left(\dot{w}_{1,xx}\right.\right.\\
&\left.\left.+ \mathrm{VCFV}_{\text{avg,no slip}}w_{1,xxx} + \frac{1}{R_{1I}^2}\dot{w}_{1,\theta\theta} - \frac{1}{R_{1I}^2}\dot{w}_1\right.\right.\\
&\left.\left.+ \mathrm{VCFV}_{\text{avg,no slip}}\frac{1}{R_{1I}^2}w_{1,x\theta\theta}\right.\right.\\
&\left.\left.- \frac{1}{R_{1I}^2}(\mathrm{VCF})V_{\text{avg,no slip}}w_{1,x} - \frac{2}{R_{1I}^2}\dot{v}_{1,\theta}\right)\right]\\
&- (-1)^i\frac{R_{1o}}{R_i}(c(w_2-w_1)+c_n(w_2-w_1)^3)\\
&- m_1\frac{R_{2o}}{R_i}\left(K_w w_2 + cv\dot{w}_2 - K_G\nabla^2 w_2\right), \qquad (21b)\\
&\frac{1}{R_i}\left[\frac{Eh}{1-\upsilon^2}\left(\frac{1}{R_i}v_{i,\theta} + \frac{w_i}{R_i} + \frac{1}{2R_i^2}(w_{i,\theta})^2\right.\right.\\
&\left.\left.+ \upsilon u_{i,x} + \frac{\upsilon}{2}{w_{i,x}}^2\right) - \frac{EhT(\alpha_\theta+\upsilon\alpha_x)}{1-\upsilon^2}\right]_{,\theta}\\
&+ \frac{1}{R_i}\left[(2\mu_s+\lambda_s)\left(\left(\frac{1}{R_i}(v_{i,\theta}+w_i)\right.\right.\right.\\
&\left.\left.\left.+ \frac{1}{2R_i^2}(w_{i,\theta})^2 - \alpha_\theta^s T\right) - \alpha_x^s T\right) + 2\tau^s\right]_{,\theta}\\
&+ \left[\frac{Eh}{2(1+\upsilon)}\left(\frac{1}{R_i}u_{i,\theta} + v_{i,x} + \frac{1}{R_i}w_{i,\theta}w_{i,x}\right)\right]_{,x}\\
&= (1-(e_0a)^2\nabla^2)\left((\rho_t h + 2\rho^s)\ddot{v}_i + m_0\rho_f\frac{R_{1I}^2}{2R_1}\ddot{v}_1\right), \qquad (21c)\\
&\left[h_{11}h\left(u_{i,x} + \frac{1}{2}w_{i,x} - \alpha_x T\right) - \zeta_{11}h\varphi_{xi,x}\right]_{,x}\\
&+ \left[h_{11}^s\left(u_{i,x} + \frac{1}{2}{w_{i,x}}^2 - \alpha_x^s T\right) - \zeta_{11}^s\varphi_{xi,x}\right]_{,x}\\
&= 0, \qquad (21d)
\end{aligned}
$$

It should be noted that a combination of electro-thermo-mechanical loading is exerted on the surface and bulk material of DWBNNT in the axial and circumferential directions, which are:

$$
\begin{aligned}
N_{xi} &= N_{xi}^M + N_{xi}^T + N_{xi}^E + N_{xi}^{sT} + N_{xi}^{sE} + 2\tau^s,\\
N_{\theta i} &= N_{\theta i}^T + N_{\theta i}^{sT} + 2\tau^s, \qquad (22)
\end{aligned}
$$

where superscript M, T and E indicate the mechanical, thermal and electric components of the load as:

$$N_{xi}^{T} = \frac{-Eh\alpha_x T}{1-\upsilon},$$

$$N_{\theta i}^{T} = \frac{-Eh\alpha_\theta T}{1-\upsilon},$$

$$N_{xi}^{sT} = -(2\mu_s + \lambda_s)\alpha_x^s T,$$

$$N_{\theta i}^{sT} = -(2\mu_s + \lambda_s)\alpha_\theta^s T,$$

$$N_{xi}^{sE} = -h_{11}^s E_{xi},$$

$$N_{xi}^{E} = -h_{11} E_{xi} h,$$

$$N_{xi}^{M} = N, \tag{23}$$

and torsional loading is neglected ($N_{x\theta i} = 0$).

The following dimensionless parameters are defined to simplify the governing equations:

$$X = \frac{x}{L}, \qquad U_i, W_i, V_i = \frac{u_i, w_i, v_i}{R_i}, \qquad \beta = \frac{h}{L},$$

$$\alpha = \frac{e_0 a}{L}, \qquad \tau = \frac{t}{L}\sqrt{\frac{E}{\rho_t}}, \qquad \varphi_{ni} = \frac{\varphi_{xi} h_{11}}{EL},$$

$$\rho = \frac{\rho_f}{\rho_t}, \qquad \bar{\rho} = \frac{\rho^s}{\rho_t L}, \qquad R_{ni} = \frac{R_i}{L},$$

$$\Delta x = \alpha_x T, \qquad \Delta\theta = \alpha_\theta T, \qquad \bar{\Delta} x = \alpha_x^s T,$$

$$\bar{\Delta}\theta = \alpha_\theta^s T, \qquad C_{vdw} = \frac{cL}{E}, \qquad C_N = \frac{c_n L^3}{E},$$

$$\mu_n = \frac{\mu}{L\sqrt{E\rho_t}}, \qquad K_{nw} = \frac{K_w L}{E}, \qquad K_{nG} = \frac{K_G}{EL},$$

$$v = V_{\text{avg,no slip}}\sqrt{\frac{\rho_t}{E}}, \qquad C_{vis} = \frac{cv}{\sqrt{E\rho_t}}, \qquad I_n = \frac{I_f}{A_1 L^2},$$

$$H = \frac{h_{11}^2}{E\zeta_{11}}, \qquad \bar{H} = \frac{h_{11}^s}{h_{11} L}, \qquad \bar{e} = \frac{\zeta_{11}^s}{\zeta_{11} L},$$

$$N_M = \frac{N}{EL}, \qquad \bar{\mu}_s = \frac{\mu_s}{EL}, \qquad \bar{\lambda}_s = \frac{\lambda_s}{EL},$$

$$tn = \frac{\tau^s}{EL}, \qquad R_{niI} = \frac{R_{iI}}{L}, \qquad R_{nio} = \frac{R_{io}}{L}. \tag{24}$$

Substituting the above dimensionless relations to Eqs. (21), yields the dimensionless motion equations.

5. Solution method

5.1. Galerkin approach

The Galerkin method is used to convert the governing equations to ordinary differential equations. So, dimensionless mechanical displacements and electric potential are assumed as:

$$U_i(X,\tau) = ui(X)Ui(\tau),$$

$$W_i(X,\tau) = wi(X)Wi(\tau),$$

$$V_i(X,\tau) = vi(X)Vi(\tau),$$

$$\varphi_{ni}(X,\tau) = \chi i(X)\kappa i(\tau), \tag{25}$$

where $Ui(\tau)$, $Wi(\tau)$, $Vi(\tau)$ and $\kappa i(\tau)$ are related to dynamical response and $ui(X)$, $vi(X)$, $wi(X)$, $\chi i(X)$ should satisfy the boundary conditions resulted from the variational process:

$$ui(X) = wi(X) = \Theta i(X) = \chi i(X) = \sin(\pi X),$$

$$\text{at} \quad X = 0, 1. \tag{26}$$

Time dependent equations are derived as follows, after substituting Eqs. (25) and (26) into a dimensionless form of Eq. (21) and applying the Galerkin method. It should be noted that through this process, electric and mechanical fields will be decoupled, considering Eq. (21d).

$$\omega^2 M\frac{d^2(Y(\bar{\tau}))}{d\bar{\tau}^2} + \omega\bar{C}\frac{d(Y(\bar{\tau}))}{d\bar{\tau}} + (K_L + K_{NL} - (N_0 + N_s\cos(2\bar{\tau}))K_g)Y = 0, \tag{27}$$

where $\bar{\tau} = \omega\tau$ is a new parameter containing the non-dimensional frequency of excitation (2ω) and:

$$N_M = N_0 + N_s\cos(2\bar{\tau}), \tag{28}$$

is substituted in Eq. (27), where N_0 is the static component of dimensionless harmonic axial load (N_M) and N_s is its dynamic component [23]. Also, M, $\bar{C}$, K_L, K_{NL} and K_g are the mass, damping, linear stiffness, nonlinear stiffness and geometric stiffness matrices, respectively, and Y is the displacement vector as:

$$M = \begin{bmatrix} m_{11} & 0 & 0 & 0 & 0 & 0 \\ 0 & m_{22} & 0 & 0 & 0 & 0 \\ 0 & 0 & m_{33} & 0 & 0 & 0 \\ 0 & 0 & 0 & m_{44} & 0 & 0 \\ 0 & 0 & 0 & 0 & m_{55} & 0 \\ 0 & 0 & 0 & 0 & 0 & m_{66} \end{bmatrix},$$

$$K_L = \begin{bmatrix} k_{11} & 0 & 0 & 0 & 0 & 0 \\ 0 & k_{22} & 0 & 0 & 0 & 0 \\ 0 & 0 & k_{33} & k_{34} & 0 & 0 \\ 0 & 0 & k_{43} & k_{44} & 0 & 0 \\ 0 & 0 & 0 & 0 & k_{55} & 0 \\ 0 & 0 & 0 & 0 & 0 & k_{66} \end{bmatrix},$$

$$\bar{C} = \begin{bmatrix} 0 & 0 & 0 & 0 & 0 & 0 \\ 0 & 0 & 0 & 0 & 0 & 0 \\ 0 & 0 & \bar{c}_{33} & 0 & 0 & 0 \\ 0 & 0 & 0 & \bar{c}_{44} & 0 & 0 \\ 0 & 0 & 0 & 0 & 0 & 0 \\ 0 & 0 & 0 & 0 & 0 & 0 \end{bmatrix},$$

$$K_{NL} = \begin{bmatrix} 0 & 0 & 0 & 0 & 0 & 0 \\ 0 & 0 & 0 & 0 & 0 & 0 \\ 0 & 0 & KN_{33} & KN_{34} & 0 & 0 \\ 0 & 0 & KN_{43} & KN_{44} & 0 & 0 \\ 0 & 0 & 0 & 0 & 0 & 0 \\ 0 & 0 & 0 & 0 & 0 & 0 \end{bmatrix},$$

$$K_g = \begin{bmatrix} 0 & 0 & 0 & 0 & 0 & 0 \\ 0 & 0 & 0 & 0 & 0 & 0 \\ 0 & 0 & kg_{33} & 0 & 0 & 0 \\ 0 & 0 & 0 & kg_{44} & 0 & 0 \\ 0 & 0 & 0 & 0 & 0 & 0 \\ 0 & 0 & 0 & 0 & 0 & 0 \end{bmatrix},$$

$$Y = [U1, U2, W1, W2, V1, V2]^T. \tag{29}$$

The components of the above matrices have been stated in Appendix A.

5.2. IHBM

IHBM represents high precision in dynamic stability analysis [22,35,36]. In this approach, (N_s^*, ω^*) are considered as known instability boundary points corresponding to the solution of Eq. (27), i.e. $Y^*(\bar{\tau})$, a neighboring instability point, is assumed as:

$$Y(\bar{\tau}) = Y^*(\bar{\tau}) + \Delta Y(\bar{\tau}),$$

$$N_s = N_s^* + \Delta N_s, \qquad \omega = \omega^* + \Delta\omega. \tag{30}$$

Linear incremental equations can be obtained by substituting Eq. (30) into Eq. (27) and neglecting higher order terms as:

$$\begin{aligned} &\omega^{*^2} M \frac{d^2(\Delta Y(\bar{\tau}))}{d\bar{\tau}^2} + \omega^* \bar{C} \frac{d(\Delta Y(\bar{\tau}))}{d\bar{\tau}} \\ &\quad + (K_L + K_N^* - (N_0 + N_s^* \cos(\bar{\tau}))K_g)\Delta Y(\bar{\tau}) \\ &\quad = R - \left(2\omega^* M \frac{d^2(Y^*(\bar{\tau}))}{d\bar{\tau}^2} + \bar{C} \frac{d(Y^*(\bar{\tau}))}{d\bar{\tau}}\right) \Delta\omega \\ &\quad + \cos(\bar{\tau}) K_g Y^*(\bar{\tau}) \Delta N_s, \end{aligned} \tag{31}$$

where:

$$\begin{aligned} R = -\Bigg[&\omega^{*^2} M \frac{d^2(Y^*(\bar{\tau}))}{d\bar{\tau}^2} + \omega^* \bar{C} \frac{d(Y^*(\bar{\tau}))}{d\bar{\tau}} \\ &+ (K_L + K_{NL}^* - (N_0 + N_s^* \cos(\bar{\tau}))K_g) Y^*(\bar{\tau}) \Bigg], \end{aligned} \tag{32}$$

is the corrective term and will be zero on the exact instability boundary points [22]. K_{NL} equals K_{NL}^* when $Y(\bar{\tau})$ is $Y^*(\bar{\tau})$, and K_N^* is:

$$K_N^* = \begin{bmatrix} 0 & 0 & 0 & 0 & 0 & 0 \\ 0 & 0 & 0 & 0 & 0 & 0 \\ 0 & 0 & kn_{33} & kn_{34} & 0 & 0 \\ 0 & 0 & kn_{43} & kn_{44} & 0 & 0 \\ 0 & 0 & 0 & 0 & 0 & 0 \\ 0 & 0 & 0 & 0 & 0 & 0 \end{bmatrix},$$

$$\begin{aligned} kn_{33} =& -\frac{K_1 K_3}{R_{n1}^3}[-6R_{n2} W2^*.W1^*.R_{n1}^2 \\ &+ 3R_{n1} R_{n2}^2 (W2^*)^2 + 3R_{n1}^3 (W1^*)^2], \\ kn_{34} =& -\frac{K_1 K_3}{R_{n1}^3}[6R_{n1} W2^*.W1^*.R_{n2}^2 \\ &- 3R_{n2} R_{n1}^2 (W1^*)^2 - 3R_{n2}^3 (W2^*)^2], \\ kn_{43} =& \frac{K_2 K_3}{R_{n2}^3}[-6R_{n2} W2^*.W1^*.R_{n1}^2 \\ &+ 3R_{n1} R_{n2}^2 (W2^*)^2 + 3R_{n1}^3 (W1^*)^2], \\ kn_{34} =& \frac{K_2 K_3}{R_{n2}^3}[6R_{n1} W2^*.W1^*.R_{n2}^2 \\ &- 3R_{n2} R_{n1}^2 (W1^*)^2 - 3R_{n2}^3 (W2^*)^2], \end{aligned} \tag{33}$$

where K_1, K_2 and K_3 are defined in Appendix A.

The principal region of instability can be determined by considering $Y^*(\bar{\tau})$ and $\Delta Y(\bar{\tau})$ as the harmonic functions with period 2π. So, Fourier series expansion is used in this method as:

$$\begin{aligned} Y_n^*(\bar{\tau}) = \sum_{i=1}^{N_h} \Bigg\{ &a_{n(2i-1)} \cos[(2i-1)\bar{\tau}] \\ &+ b_{n(2i-1)} \sin[(2i-1)\bar{\tau}] \Bigg\} = \eta . A_n, \end{aligned}$$

$$n = 1, 2, \cdots, 6,$$

$$\Delta Y_n(\bar{\tau}) = \sum_{i=1}^{N_h} \Big\{ \Delta a_{n(2i-1)} \cos[(2i-1)\bar{\tau}] + \Delta b_{n(2i-1)} \sin[(2i-1)\bar{\tau}] \Big\} = \eta.\Delta A_n, \tag{34}$$

where N_h is a large integer, and:

$$\eta = [\cos(\bar{\tau}), \cos(3\bar{\tau}), \cdots, \cos[(2N_h-1)\bar{\tau}], \sin(\bar{\tau}), \sin(3\bar{\tau}), \cdots, \sin[(2N_h-1)\bar{\tau}]],$$

$$A_n = [a_{n1}, a_{n3}, \cdots, a_{n(2N_h-1)}, b_{n1}, b_{n3}, \cdots, b_{n(2N_h-1)}]^T,$$

$$\Delta A_n = [\Delta a_{n1}, \Delta a_{n3}, \cdots, \Delta a_{n(2N_h-1)}, \Delta b_{n1}, \Delta b_{n3}, \cdots, \Delta b_{n(2N_h-1)}]^T,$$

$$n = 1, 2, \cdots, 6. \tag{35}$$

On the other hand:

$$Y^* = \bar{Q}.A, \qquad \Delta Y = \bar{Q}.\Delta A, \tag{36}$$

where:

$$\bar{Q} = \begin{bmatrix} \eta & 0 & 0 & 0 & 0 & 0 \\ 0 & \eta & 0 & 0 & 0 & 0 \\ 0 & 0 & \eta & 0 & 0 & 0 \\ 0 & 0 & 0 & \eta & 0 & 0 \\ 0 & 0 & 0 & 0 & \eta & 0 \\ 0 & 0 & 0 & 0 & 0 & \eta \end{bmatrix},$$

$$A = \begin{bmatrix} A_1 \\ A_2 \\ A_3 \\ A_4 \\ A_5 \\ A_6 \end{bmatrix}, \qquad \Delta A = \begin{bmatrix} \Delta A_1 \\ \Delta A_2 \\ \Delta A_3 \\ \Delta A_4 \\ \Delta A_5 \\ \Delta A_6 \end{bmatrix}. \tag{37}$$

Inserting Eq. (36) into Eq. (31) and applying the Galerkin method results in:

$$\int_0^{2\pi} \delta(\Delta Y(\bar{\tau}))^T . \Big[\omega^{*^2} M \frac{d^2(\Delta Y(\bar{\tau}))}{d\bar{\tau}^2} + \omega^* \bar{C} \frac{d(\Delta Y(\bar{\tau}))}{d\bar{\tau}} + (K_L + K_N^* - (N_0 + N_s^* \cos(\bar{\tau}))K_g)\Delta Y(\bar{\tau}) \Big] d\bar{\tau}$$

$$= \int_0^{2\pi} \delta(\Delta Y(\bar{\tau}))^T . \Big[R - \Big(2\omega^* M \frac{d^2(Y^*(\bar{\tau}))}{d\bar{\tau}^2} + \bar{C} \frac{d(Y^*(\bar{\tau}))}{d\bar{\tau}} \Big) \Delta\omega + \cos(\bar{\tau}) K_g Y^*(\bar{\tau}) \Delta N_s \Big] d\bar{\tau}. \tag{38}$$

A linear system of equations containing ΔA, $\Delta\omega$ and ΔN_s can be obtained as:

$$S1.\Delta A = RR + S2\Delta\omega + S3\Delta N_s, \tag{39}$$

where:

$$S1 = \omega^{*2} H_1 + \omega^* H_2 + H_3 + H_5 + H_6,$$

$$S2 = -(2\omega^* H_1 + H_2).A,$$

$$S3 = H_7.A,$$

$$RR = -\left(\omega^{*2} H_1 + \omega^* H_2 + H_3 + H_4 + H_5\right).A,$$

$$H_1 = \int_0^{2\pi} \bar{Q}^T M \frac{d^2\bar{Q}}{d\bar{\tau}^2} d\bar{\tau},$$

$$H_2 = \int_0^{2\pi} \bar{Q}^T C \frac{d\bar{Q}}{d\bar{\tau}} d\bar{\tau},$$

$$H_3 = \int_0^{2\pi} \bar{Q}^T K_L \bar{Q} d\bar{\tau},$$

$$H_4 = \int_0^{2\pi} \bar{Q}^T K_{NL}^* \bar{Q} d\bar{\tau},$$

$$H_5 = -\int_0^{2\pi} \bar{Q}^T (N_0 + N_s^* \cos(\bar{\tau})) K_g \bar{Q} d\bar{\tau},$$

$$H_6 = \int_0^{2\pi} \bar{Q}^T K_N^* \bar{Q} d\bar{\tau},$$

$$H_7 = -\int_0^{2\pi} \bar{Q}^T \cos(\bar{\tau}) K_g \bar{Q} d\bar{\tau}. \tag{40}$$

The following procedure should be done to derive dynamic instability regions.

Step 1: Linear free vibration analysis. After neglecting the nonlinear stiffness matrix and dynamic axial load, Eq. (27) will be reduced to:

$$\omega^2 M \frac{d^2(Y(\bar{\tau}))}{d\bar{\tau}^2} + \omega\bar{C} \frac{d(Y(\bar{\tau}))}{d\bar{\tau}} + K_L Y = 0. \tag{41}$$

This equation is a generalized eigenvalue problem and could be changed into the standard form [17,37]. Eq. (41) can be written in state-space representation:

$$\dot{Z} = BZ, \tag{42}$$

in which B and Z are defined as:

$$B = \begin{bmatrix} 0 & I \\ -M^{-1}K_L & -M^{-1}\bar{C} \end{bmatrix}, \qquad Z = \begin{Bmatrix} Y \\ \dot{Y} \end{Bmatrix}, \tag{43}$$

where 0 and I represent zero and unitary matrices, respectively.

The fundamental frequency and corresponding eigenvector in a linear problem will be considered as primary values of ω^* and vector A in Eq. (39).

Step 2: Static buckling analysis. By neglecting inertia terms, the dynamic component of axial load (N_s), and assuming $N_0 = P_{cr}$, Eq. (27) will be reduced to:

$$(K_L + K_{NL} - P_{cr}K_g)Y = 0, \tag{44}$$

where P_{cr} stands for dimensionless static critical buckling load and can be determined by solving the above eigenvalue problem. N_0 and N_s will be considered as:

$$N_0 = \alpha_1 P_{cr}, \qquad N_s = \alpha_2 P_{cr}, \tag{45}$$

where α_1 and α_2 are the static and dynamic load factors.

Step 3: Dynamic instability analysis. Eq. (39) denotes a linear system with $2N$ equations and $2N+2$ unknowns (ΔA, $\Delta\omega$, ΔN_s). One of the components of vector A is chosen as a reference constant, with its corresponding increment set to zero (in this analysis $a_{31} = 1$ and $\Delta a_{31} = 0$) and ΔN_s (or $\Delta\omega$) is specified as an active increment. Other unknowns can be derived from Eq. (39) considering initial values described in previous steps. New values for A and ω can be calculated as $a_1 + \Delta a_1, b_1 + \Delta b_1, \cdots, \omega^* + \Delta\omega$. This procedure will be continued until the value of RR is small enough, then a new iterative step begins, giving an active increment ΔN_s to N_s.

Finally, the first boundary of DIR will be determined. The other boundary of DIR can be specified considering b_{31} as a reference constant ($b_{31} = a_{31}$, $\Delta b_{31} = 0$) and repeating Step 3.

6. Results and discussion

In this paper, the dynamic stability of DWBNNT conveying viscose fluid is investigated considering surface stress effects. DWBNNT is under periodic excitation in a thermal environment and embedded in a visco-Pasternak medium. Hamilton's principle is used to derive nonlinear governing equations based on nonlocal shell theory. IHBM is utilized to derive dynamic instability regions. The results of this study are based on the following geometric and mechanical data for the bulk material [17,38,39]:

$$R_1 = 11.43 \text{ nm}, \qquad R_2 = 12.31 \text{ nm},$$

$$\frac{L}{R_1} = 10, \qquad h = 0.075 \text{ nm},$$

$$\alpha_x = 1.2 \times 10^{-6} \ \frac{1}{^\circ\text{C}},$$

$$\alpha_\theta = 0.6 \times 10^{-6} \ \frac{1}{^\circ\text{C}}, \qquad T = 20 \ ^\circ\text{C},$$

$$E = 1.8 \text{ Tpa}, \qquad \rho_t = 3487 \ \frac{\text{kg}}{\text{m}^3},$$

$$\rho_f = 1000 \ \frac{\text{kg}}{\text{m}^3},$$

$$\mu_0 = 0.653 \times 10^{-3} \text{ Pa.s},$$

$$K_w = 8.9995035 \times 10^{17} \ \frac{\text{N}}{\text{m}^3},$$

$$K_G = 2.071273 \ \frac{\text{N}}{\text{m}},$$

$$cv = 4.491989398 \times 10^{-7} \ \frac{\text{N.s}}{\text{m}^3},$$

$$c = 9.91866693 \times 10^{19} \ \frac{\text{N}}{\text{m}^3},$$

$$c_n = 2.201667 \times 10^{31} \ \frac{\text{N}}{\text{m}^5},$$

$$h_{11} = 0.95 \ \frac{\text{C}}{\text{m}^2}, \qquad \zeta_{11} = 0.9824 \times 10^{-8} \ \frac{\text{F}}{\text{m}}.$$

In Figure 2, the results of this study are compared with the results of [24] for DIR of SWCNT. The effects of surface stress, vdW force, fluid flowing, shear and the damping constant of the medium are neglected in this figure. As can be seen, the two analyses agree well and show similar results.

In Figures 3 to 12, DIRs of DWBNNT are shown and the effects of various parameters on them are discussed. The vertical axis indicates Ω, which is the ratio of nonlinear to linear frequency ($\Omega = \omega_{NL}/\omega_L$), and the horizontal axis represents the dynamic load factor (α_2).

Figure 3 depicts the effect of the nonlocal parameter on DIR of DWBNNT. As can be seen, increasing the nonlocal parameter shifts the DIR to the lower frequency zone. Increasing the nonlocal parameter increases the length of the $b-N$ bond and, subsequently, the stiffness of DWBNNT decreases.

In Figure 4, the DIR of DWBNNT is shown for different dimensionless flow velocities. Increasing the

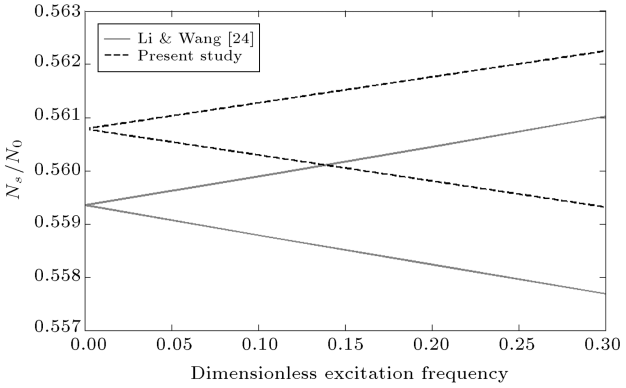

Figure 2. Comparison between the results of present study and the results of [24] for SWCNT.

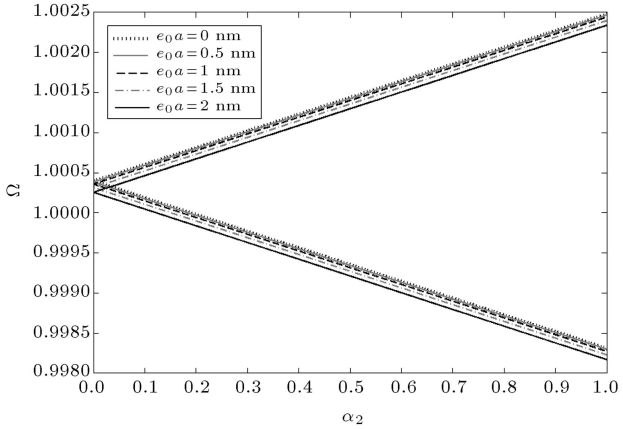

Figure 3. The effect of nonlocality on DIR of a DWBNNT.

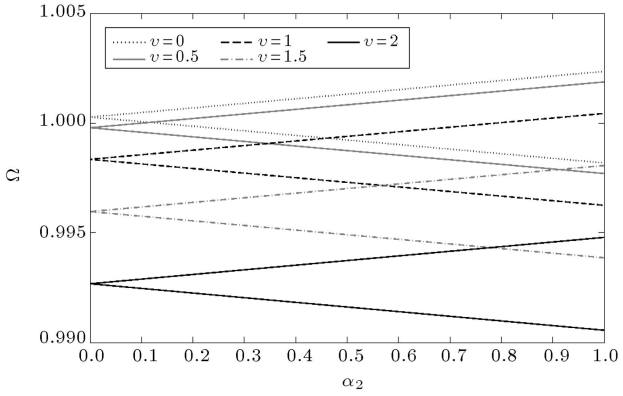

Figure 4. The effect of fluid velocity on DIR of a DWBNNT.

fluid velocity through the inner nanotube decreases the frequency. Shifting the DIRs is more obvious in higher flow velocities. Flowing fluid through the DWBNNT exerts compressive axial load, and for higher velocities, the magnitude of this load increases. So, increasing flow velocity results in a decrease in frequency.

Figure 5 indicates the effect of Knudsen number on DIR of DWBNNT. As shown in this figure, continuum fluid ($K_n = 0$) predicts the highest frequency zone. Considering fluid with higher Knudsen number results in shifting the DIR to the lower frequency zone very slowly. In dynamic stability analysis, the small-size effect of liquid nanoflow can be ignored because the Knudsen number has small values. As the Knudsen number increases, the mean free path of the liquid molecules increases and results in lower stiffness.

Figure 6 represents the effect of viscosity on the DIR of DWBNNT. When viscosity is neglected, the DIR of DWBNNT consists of two different boundaries, but considering viscosity results in one integrated path with a U-turn portion. This result can be seen in [36], as the damping coefficient effect on DIR is studied.

Figure 7 shows that DWBNNT's DIR shifts to a

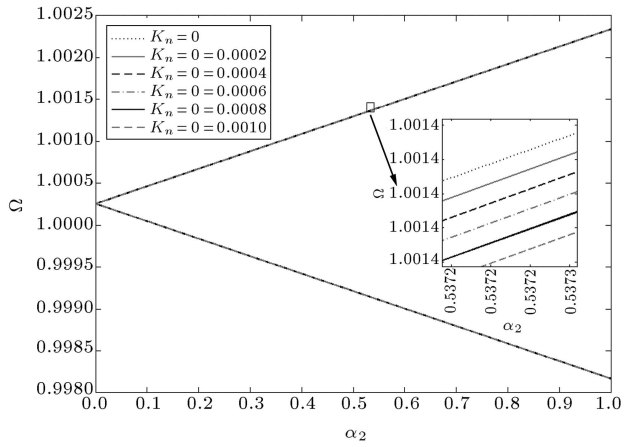

Figure 5. The effect of Knudsen number on DIR of a DWBNNT.

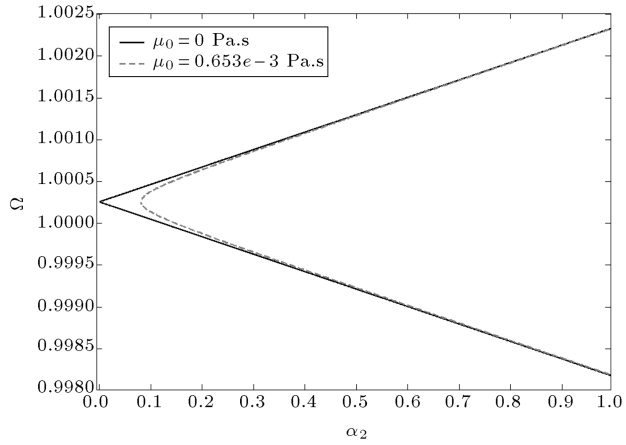

Figure 6. The effect of viscosity on DIR of a DWBNNT.

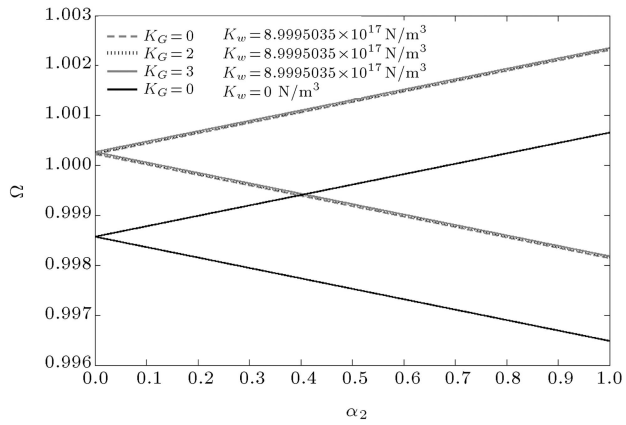

Figure 7. The effect of surrounding medium on DIR of a DWBNNT.

higher frequency zone as the medium becomes stronger. Considering the Winkler medium leads to a higher frequency zone, very drastically, because of the Winkler coefficient's large value. Also, by considering the Pasternak medium, DIR acts in the same manner with slower changes.

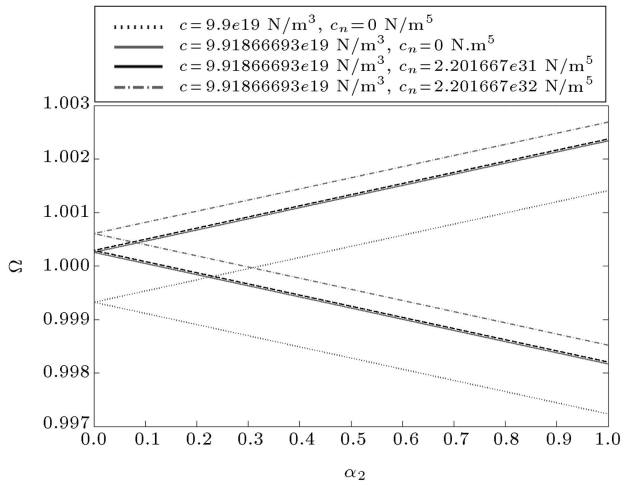

Figure 8. The effect of vdW forces on DIR of a DWBNNT.

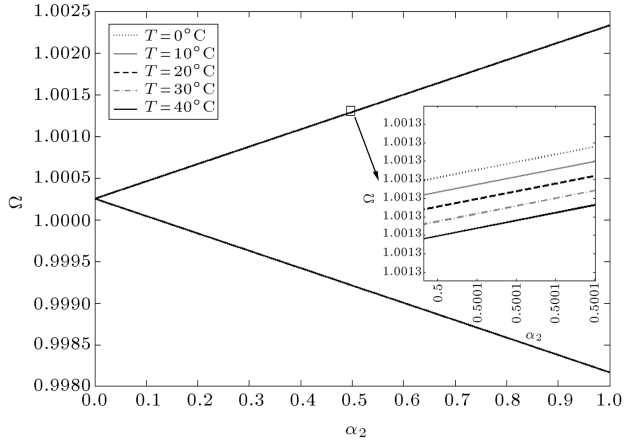

Figure 9. The effect of high temperature environment on DIR of a DWBNNT.

In Figure 8, the vdW effect is represented. This figure shows that considering vdW effects results in a higher frequency zone. Also, considering the nonlinear term of vdW forces has an important role in DIRs. As shown in this figure, considering this effect moves the origin of DIR towards the higher frequency zone.

Figure 9 illustrates the effect of temperature change on the DIR of DWBNNT considering high temperature environments. At high temperatures (α_x, $\alpha_\theta \succ 0$), an increase in temperature change leads the DIR to the lower frequency zone. As shown in this figure, the effect of temperature change on DIR is very negligible. Drastic thermal changes result in reducing the strength of the $b - N$ bond, so, limited thermal changes should be applied. According to Eq. (23), increasing temperature induces compressive load in DWBNNT and, subsequently, a decrease in frequency is not unexpected.

The effect of static load factor (α_1) on the DIR of DWBNNT is shown in Figure 10. It is found that increasing the static load factor shifts the DIR towards

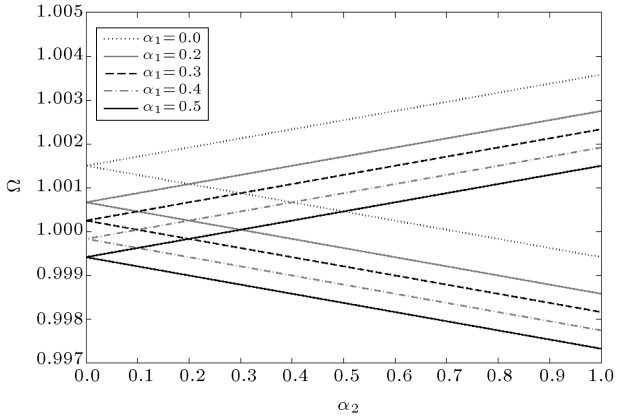

Figure 10. The effect of static load factor on DIR of a DWBNNT.

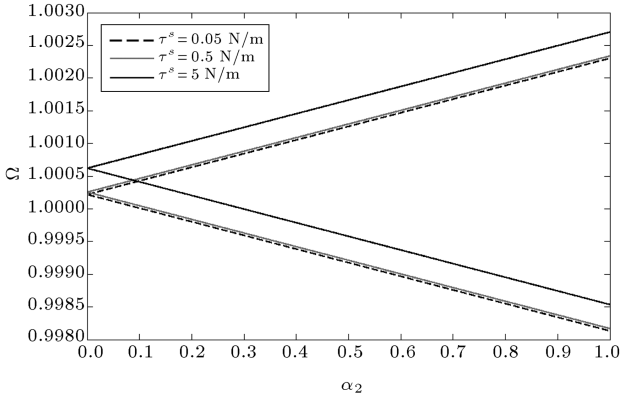

Figure 11. The effect of residual surface stress on DIR of a DWBNNT.

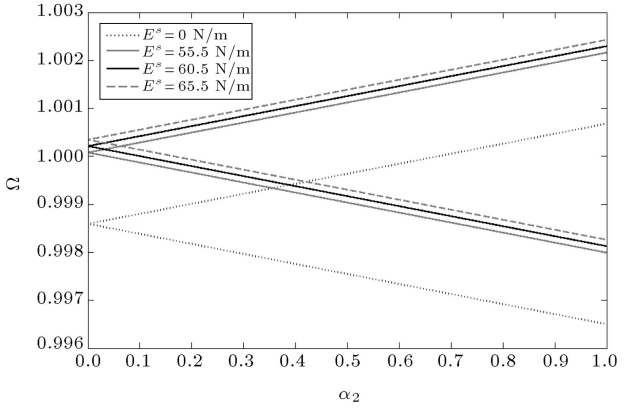

Figure 12. The effect of surface modulus on DIR of a DWBNNT.

the origin. Considering Eq. (45), axial loading with a higher static load factor is relevant to a higher static compressive load, so, this result is reasonable.

Finally, the effect of surface parameters on the DIR of DWBNNT is shown in Figures 11 and 12. According to Figure 11, a higher frequency zone refers to higher residual surface stress. Based on [25], positive values of τ^s make DWBNNT stiffer, due to applying

tensile loading. The effect of surface modulus on the DIR of DWBNNT is presented in Figure 12. As the surface modulus increases, the DIR moves to a higher frequency zone due to stiffness increasing.

7. Conclusion

By applying IHBM and considering the charge equation, the dynamic stability of embedded DWBNNT conveying viscous fluid was investigated using a nonlocal shell model. The effects of the surrounding elastic medium and nonlinear vdW forces between the inner and outer nanotubes were taken into account. Also, the effect of fluid-DWBNNT interaction was studied considering slip boundary conditions. The following conclusions may be made from the results:

- Considering surface effects in DWBNNT is very significant; increasing residual surface stress and surface modulus shift DIR to a higher frequency zone.
- Increasing the nonlocal parameter shifts the DIR to the lower frequency zone.
- Considering fluid velocity and Knudsen number results in shifting the DIR to the lower frequency zone, and, for liquid fluid, the effect of Knudsen number can be vanished.
- Considering viscosity results in one integrated path for DIR instead of different boundaries.
- Considering the surrounding medium results in a higher frequency zone.
- Considering vdW effects results in a higher frequency zone.
- At high temperatures, an increase in temperature change shifts the DIR to the lower frequency zone.
- It is obvious that increasing the static load factor shifts DIR to a higher frequency zone.

Acknowledgments

The author would like to thank the reviewers for their comments and suggestions to improve the clarity of this article. The authors are grateful to the University of Kashan for supporting this work by Grant No. 65475/48. They would also like to thank the Iranian Nanotechnology Development Committee for their financial support.

References

1. Salehi-Khojin, A. and Jalili, N. "Buckling of boron nitride nanotube reinforced piezoelectric polymeric composites subject to combined electro-thermo-mechanical loadings", *Compos. Sci. Tech.*, **68**(6), pp. 1489-1501 (2008).
2. Païdoussis, M.P., Chan, S.P. and Misra, A.K. "Dynamics and stability of coaxial cylindrical shells containing flowing fluid", *J. Sound and Vib.*, **97**(2), pp. 201-235 (1984).
3. Païdoussis, M.P., *Fluid-Structure Interactions: Slender Structures and Axial Flow*, Academic Press, London (1998).
4. Amabili, M., Pellicano, F. and Païdoussis, M.P. "Nonlinear dynamics and stability of circular cylindrical shells conveying flowing fluid", *Comput. Struct.*, **80**(9-10), pp. 899-906 (2002).
5. Amabili, M., Karagiozis K. and Païdoussis, M.P. "Effect of geometric imperfections on non-linear stability of circular cylindrical shells conveying fluid", *Int. J. Non-Linear Mech.*, **44**(3), pp. 276-289 (2009).
6. Khosravian, N. and Rafii-Tabar, H. "Computational modelling of the flow of viscous fluids in carbon nanotubes", *J. Phys. D: Appl. Phys.*, **40**(22), pp. 7046-7052 (2007).
7. Yan, Y., He, X.Q. and Zhang, L.X. "Dynamic behavior of triple-walled carbon nanotubes conveying fluid", *J. Sound and Vib.*, **319**(3-5), pp. 1003-1018 (2009).
8. Lee, H.L. and Chang, W.J. "Vibration analysis of fluid-conveying double-walled carbon nanotubes based on nonlocal elastic theory", *J. Phys. Condens. Matter*, **21**(11), pp. 115302-1:5 (2009).
9. Rasekh, M. and Khadem, S.E. "Nonlinear vibration and stability analysis of axially loaded embedded carbon nanotubes conveying fluid", *J. Phys. D: Appl. Phys.*, **42**(13), pp. 135112-1:8 (2009).
10. Wang, L. and Ni, Q. "A reappraisal of the computational modelling of carbon nanotubes conveying viscous fluid", *Mech. Res. Commun.*, **36**(7), pp. 833-837 (2009).
11. Wang, L. "Dynamical behaviors of double-walled carbon nanotubes conveying fluid accounting for the role of small length scale", *Comput. Mat. Sci.*, **45**(2), pp. 584-588 (2009).
12. Yan, Y., Wang, W.Q. and Zhang, L.X. "Noncoaxial vibration of fluid-filled multi-walled carbon nanotubes", *Appl. Math. Model.*, **34**(1), pp. 122-128 (2010).
13. Ghavanloo, E., Daneshmand, F. and Rafiei, M. "Vibration and instability analysis of carbon nanotubes conveying fluid and resting on a linear viscoelastic Winkler foundation", *Physica E*, **42**(9), pp. 2218-2224 (2010).
14. Ke, L.L. and Wang, Y.S. "Flow-induced vibration and instability of embedded double-walled carbon nanotubes based on a modified couple stress theory", *Physica E*, **43**(5), pp. 1031-1039 (2011).
15. Farshidianfar, A. and Soltani, P. "Nonlinear flow-induced vibration of a SWCNT with a geometrical imperfection", *Comput. Mat. Sci.*, **53**(1), pp. 105-116 (2012).

16. Rashidi, V., Mirdamadi, H.R. and Shirani, E. "A novel model for vibrations of nanotubes conveying nanoflow", *Comput. Mat. Sci.*, **51**(1), pp. 347-352 (2012).

17. Khodami Maraghi, Z., Ghorbanpour Arani, A., Kolahchi, R., Amir, S. and Bagheri, M.R. "Nonlocal vibration and instability of embedded DWBNNT conveying viscose fluid", *Compos. Part B, Eng.*, **45**(1), pp. 423-432 (2013).

18. Ghorbanpour Arani, A., Shajari, A.R., Atabakhshian, V., Amir, S. and Loghman, A. "Nonlinear dynamical response of embedded fluid-conveyed micro-tube reinforced by BNNTs", *Compos. Part B, Eng.*, **44**(1), pp. 424-432 (2013).

19. Ghorbanpour Arani, A., Zarei, M.S., Amir, S. and Khodami Maraghi, Z. "Nonlinear nonlocal vibration of embedded DWCNT conveying fluid using shell model", *Physica B*, **410**(0), pp. 188-196 (2013).

20. Ghorbanpour Arani, A., Kolahchi, R. and Vossough, H. "Nonlocal wave propagation in an embedded DWBNNT conveying fluid via strain gradient theory", *Physica B*, **407**(21), pp. 4281-4286 (2012).

21. Lim, C.W. "On the truth of nanoscale for nanobeams based on nonlocal elastic stress field theory: Equilibrium, governing equation and static deflection", *Appl. Math. Mech.*, **31**, pp. 37-54 (2010).

22. Ansari, R., Gholami, R. and Sahmani, S. "On the dynamic stability of embedded single-walled carbon nanotubes including thermal environment effects", *Scientia Iranica*, **19**(3), pp. 919-925 (2012).

23. Fu, Y., Bi, R. and Zhang, P. "Nonlinear dynamic instability of double-walled carbon nanotubes under periodic excitation", *Acta Mech. Solida Sin.*, **22**(3), pp. 206-212 (2009).

24. Li, H.B. and Wang, X. "Effect of small scale on the dynamic characteristic of carbon nanotubes under axially oscillating loading", *Physica E*, **46**, pp. 198-205 (2012).

25. Gurtin, M.E. and Murdoch, A.I. "A continuum theory of elastic material surface", *Arch. Ration. Mech. An.*, **57**(4), pp. 291-323 (1975).

26. Ansari, R. and Sahmani, S. "Bending behavior and buckling of nanobeams including surface stress effects corresponding to different beam theories", *Int. J. Eng. Sci.*, **49**(11), pp. 1244-1255 (2011).

27. Assadi, A. and Farshi, B. "Vibration characteristics of circular nanoplates", *J. Appl. Phys.*, **108**(7), pp. 074312-074315 (2010).

28. Wang, L. "Vibration analysis of fluid-conveying nanotubes with consideration of surface effects", *Physica E*, **43**(1), pp. 437-439 (2010).

29. Wang, L. "Surface effect on buckling configuration of nanobeams containing internal flowing fluid A nonlinear analysis", *Physica E*, **44**(4), pp. 808-812 (2012).

30. Lei, X.W., Natsuki, T., Shi, J.X. and Ni, Q.Q. "Surface effects on the vibrational frequency of double-walled carbon nanotubes using the nonlocal Timoshenko beam model", *Compos. Part B: Eng.*, **43**(1), pp. 64-69 (2012).

31. Ghorbanpour Arani, A., Amir, S., Shajari, A.R. and Mozdianfard, M.R. "Electro-thermo-mechanical buckling of DWBNNTs embedded in bundle of CNTs using nonlocal piezoelasticity cylindrical shell theory", *Compos. Part B: Eng.*, **43**(2), pp. 195-203 (2012).

32. Ansari, R. and Sahmani, S. "Surface stress effects on the free vibration behavior of nanoplates", *Int. J. Eng. Sci.*, **49**(11), pp. 1204-1215 (2011).

33. Lu, P., He, L.H., Lee, H.P. and Lu, C. "Thin plate theory including surface effects", *Int. J. Solids and Struct.*, **43**(16), pp. 4631-4647 (2006).

34. Ke, L.L., Wang, Y.S. and Wang, Z.D. "Nonlinear vibration of the piezoelectric nanobeams based on the nonlocal theory", *Compos. Struct.*, **94**(6), pp. 2038-2047 (2012).

35. Fu, Y.M., Zhang, J. and Bi, R.G. "Analysis of the nonlinear dynamic stability for an electrically actuated viscoelastic microbeam", *Microsys. Tech.*, **15**(5), pp. 763-769 (2009).

36. Wu, G.Y. "The analysis of dynamic instability on the large amplitude vibrations of a beam with transverse magnetic fields and thermal loads", *J. Sound and Vib.*, **302**(1-2), pp. 167-177 (2007).

37. Amabili, M., *Nonlinear Vibrations and Stability of Shells and Plates*, Cambridge University Press, New York (2008).

38. Rafiei, M., Mohebpour, S.R. and Daneshmand, F. "Small-scale effect on the vibration of non-uniform carbon nanotubes conveying fluid and embedded in viscoelastic medium", *Physica E*, **44**(7-8), pp. 1372-1379 (2012).

39. Ghorbanpour Arani, A., Roudbari, M.A. and Amir, S. "Nonlocal vibration of SWBNNT embedded in bundle of CNTs under a moving nanoparticle", *Physica B*, **407**(17), pp. 3646-3653 (2012).

Appendix A

$$F_1 = \frac{1}{-1+v^2}, \qquad F_2 = v^2,$$

$$m_{11} = \frac{\pi}{4R_{n1}^2}\left(\alpha^2 + R_{n1}^2 + \pi^2\alpha^2 R_{n1}^2\right) \left(2R_{n1}\beta + 4R_{n1}\bar{\rho} + \rho R_{n1I}^2\right),$$

$$m_{22} = \frac{\pi}{2R_{n2}}(R_{n2}^2 + R_{n2}^2\pi^2\alpha^2 + \alpha^2)(2\bar{\rho} + \beta),$$

$$
\begin{aligned}
m_{33} =& -\frac{1}{12}\frac{\pi\bar{\rho}\beta^2F_1(R_{n1}^2\pi^2+1)\upsilon}{R_{n1}}\\
&-\frac{\pi F_1}{48R_{n1}^4}\Big(-2R_{n1}^5\pi^4\beta^3\alpha^2-24R_{n1}^5\pi^2\beta\alpha^2\\
&-4R_{n1}^5\pi^2\beta^2\bar{\rho}-48R_{n1}^5\pi^2\bar{\rho}\alpha^2+3\rho R_{n1I}^4\alpha^2F_2\\
&+12\rho R_{n1I}^2F_2R_{n1}^4+24\alpha^2\beta F_2R_{n1}^3+8\bar{\rho}\beta^2F_2R_{n1}^3\\
&+2\beta^3\alpha^2F_2R_{n1}+3\rho R_{n1I}^4F_2R_{n1}^2+48\bar{\rho}\alpha^2F_2R_{n1}^3\\
&-4\bar{\rho}\beta^2\alpha^2R_{n1}+24R_{n1}^5\beta F_2-3\rho R_{n1I}^4R_{n1}^2\\
&+48R_{n1}^5\bar{\rho}F_2-48\bar{\rho}\alpha^2R_{n1}^3-3\rho R_{n1I}^4\alpha^2\\
&-4\bar{\rho}\beta^2R_{n1}^3+2\beta^3F_2R_{n1}^3-12\rho R_{n1I}^2R_{n1}^4\\
&-24\alpha^2\beta R_{n1}^3-2\beta^3\alpha^2R_{n1}+8\pi^2\bar{\rho}\beta^2\alpha^2F_2R_{n1}^3\\
&+3\pi^4\rho R_{n1I}^4\alpha^2F_2R_{n1}^4+12\pi^2\rho R_{n1I}^2\alpha^2F_2R_{n1}^4\\
&+4R_{n1}^5\pi^4\beta^2\bar{\rho}\alpha^2F_2+6\pi^2\rho R_{n1I}^4\alpha^2F_2R_{n1}^2\\
&+12\rho R_{n1I}^2\alpha^2F_2R_{n1}^2+4\bar{\rho}\beta^2\alpha^2F_2R_{n1}\\
&+2R_{n1}^5\pi^4\beta^3\alpha^2F_2+24R_{n1}^5\pi^2\beta\alpha^2F_2\\
&+3\pi^2\rho R_{n1I}^4F_2R_{n1}^4+8R_{n1}^5\pi^2\beta^2\bar{\rho}F_2\\
&+48R_{n1}^5\pi^2\bar{\rho}\alpha^2F_2-12\pi^2\rho R_{n1I}^2\alpha^2R_{n1}^4\\
&-3\pi^4\rho R_{n1I}^4\alpha^2R_{n1}^4-4R_{n1}^5\pi^4\beta^2\bar{\rho}\alpha^2\\
&+4\pi^2\beta^3\alpha^2F_2R_{n1}^3-8\pi^2\bar{\rho}\beta^2\alpha^2R_{n1}^3\\
&-6\pi^2\rho R_{n1I}^4\alpha^2R_{n1}^2-24\beta R_{n1}^5-48R_{n1}^5\bar{\rho}\\
&-2\beta^3R_{n1}^3-2R_{n1}^5\pi^2\beta^3-12\rho R_{n1I}^2\alpha^2R_{n1}^2\\
&-4\pi^2\beta^3\alpha^2R_{n1}^3+2R_{n1}^5\pi^2\beta^3F_2\\
&-3\pi^2\rho R_{n1I}^4R_{n1}^4\Big),
\end{aligned}
$$

$$
\begin{aligned}
m_{44} =& -\frac{1}{12}\frac{\pi\bar{\rho}\beta^2F_1(R_{n2}^2\pi^2+1)\upsilon}{R_{n2}}\\
&-\frac{\pi F_1}{24R_{n2}^3}\Big(12R_{n2}^4\beta F_2+2\bar{\rho}\beta^2\alpha^2F_2\\
&-2\bar{\rho}\beta^2\alpha^2+\beta^3\alpha^2F_2-\beta^3\alpha^2-24R_{n2}^4\beta^2\alpha^2\bar{\rho}\\
&-R_{n2}^4\pi^4\beta^3\alpha^2-2R_{n2}^4\pi^2\bar{\rho}\beta^2-12R_{n2}^4\pi^2\alpha^2\beta\\
&+R_{n2}^4\pi^2\beta^3F_2-2\pi^2\beta^3\alpha^2R_{n2}^2+24\ bar\rho\alpha^2F_2R_{n2}^2\\
&+4\bar{\rho}\beta^2F_2R_{n2}^2+12\alpha^2\beta F_2R_{n2}^2\\
&+2R_{n2}^4\pi^4\bar{\rho}\beta^2\alpha^2F_2+4\pi^2\bar{\rho}\beta^2\alpha^2F_2R_{n2}^2\\
&-12\alpha^2\beta R_{n2}^2-24\bar{\rho}\alpha^2R_{n2}^2-R_{n2}^4\pi^2\beta^3\\
&+24R_{n2}^4\bar{\rho}F_2-2\bar{\rho}\beta^2R_{n2}^2+\beta^3F_2R_{n2}^2\\
&+2\pi^2\beta^3\alpha^2F_2R_{n2}^2-4\pi^2\bar{\rho}\beta^2\alpha^2R_{n2}^2\\
&+24R_{n2}^4\pi^2\alpha^2\bar{\rho}F_2+R_{n2}^4\pi^4\beta^3\alpha^2F_2\\
&+4R_{n2}^4\pi^2\bar{\rho}\beta^2F_2+12R_{n2}^4\pi^2\alpha^2\beta F_2\\
&-2R_{n2}^4\pi^4\bar{\rho}\beta^2\alpha^2-\beta^3R_{n2}^2-24R_{n2}^4\bar{\rho}\\
&-12R_{n2}^4\beta\Big),
\end{aligned}
$$

$$
\begin{aligned}
m_{55} =& \frac{\pi}{4R_{n1}^2}(\alpha^2+R_{n1}^2+\pi^2\alpha^2R_{n1}^2)\\
&(2R_{n1}\beta+4R_{n1}\bar{\rho}+\rho R_{n1I}^2),
\end{aligned}
$$

$$
m_{66} = \frac{\pi}{2R_{n2}}(\alpha^2+R_{n2}^2+\pi^2\alpha^2R_{n2}^2)(\beta+2\bar{\rho}),
$$

$$
\begin{aligned}
\bar{c}_{33} =& -\frac{\pi\mu_nF_1}{4R_{n1}^2}\Big(\pi^2R_{n1I}^2F_2R_{n1}^2+2F_2R_{n1}^2\\
&+\pi^2R_{n1I}^2\alpha^2F_2-2\alpha^2-\pi^2R_{n1I}^2R_{n1}^2\\
&-\pi^2R_{n1I}^2\alpha^2-\pi^4R_{n1I}^2\alpha^2R_{n1}^2-2R_{n1}^2\\
&-2\pi^2\alpha^2R_{n1}^2+\pi^4R_{n1I}^2\alpha^2F_2R_{n1}^2\\
&+2\alpha^2F_2+2\pi^2\alpha^2F_2R_{n1}^2\Big),
\end{aligned}
$$

$$
\begin{aligned}
\bar{c}_{44} =& -\frac{\pi R_{n2o}C_{vis}F_1}{2R_{n2}^2}\Big(-R_{n2}^2+F_2R_{n2}^2\\
&+\pi^2\alpha^2F_2R_{n2}^2-R_{n2}^2\pi^2\alpha^2-\alpha^2+\alpha^2F_2\Big),
\end{aligned}
$$

$$
\begin{aligned}
kg_{33} =& -\frac{F_1\pi^3}{2R_{n1}}\Big(-R_{n1}^2-\alpha^2-\pi^2\alpha^2R_{n1}^2\\
&+\pi^2\alpha^2F_2R_{n1}^2+F_2R_{n1}^2+\alpha^2F_2\Big),
\end{aligned}
$$

$$
\begin{aligned}
kg_{44} =& -\frac{F_1\pi^3}{2R_{n2}}\Big(-R_{n2}^2-\alpha^2-\pi^2\alpha^2R_{n2}^2\\
&+\pi^2\alpha^2F_2R_{n2}^2+F_2R_{n2}^2+\alpha^2F_2\Big),
\end{aligned}
$$

$$
k_{11} = \frac{\pi\beta\upsilon F_1}{4R_{n1}}+\frac{\pi F_1}{4(\bar{e}+\beta)R_{n1}}\Big[2R_{n1}^2\pi^2(2\bar{\mu}_s+\bar{\lambda}_s)F_2\bar{e}
$$

$$
\begin{aligned}
&+2R_{n1}^2\pi^2(2\bar{\mu}_s+\bar{\lambda}_s)F_2\beta+2\pi^2HR_{n1}^2\bar{H}^2F_2\\
&+4\pi^2HR_{n1}^2\bar{H}^2F_2\beta+2\pi^2HR_{n1}^2\beta^2F_2\\
&-4\pi^2HR_{n1}^2\beta\bar{H}-2\pi^2HR_{n1}^2\beta^2-2\pi^2HR_{n1}^2\bar{H}^2\\
&-2R_{n1}^2\pi^2\beta\bar{e}-2R_{n1}^2\pi^2\beta^2-\beta\bar{e}-\beta^2\\
&-2R_{n1}^2\pi^2(2\bar{\mu}_s+\bar{\lambda}_s)\bar{e}-2R_{n1}^2\pi^2(2\bar{\mu}_s+\bar{\lambda}_s)\beta\Big],
\end{aligned}
$$

$$
\begin{aligned}
k_{22}=&\frac{\pi\beta\upsilon F_1}{4R_{n2}}+\frac{\pi F_1}{4(\bar{e}+\beta)R_{n2}}\Big[2R_{n2}^2\pi^2(2\bar{\mu}_s+\bar{\lambda}_s)F_2\bar{e}\\
&+2R_{n2}^2\pi^2(2\bar{\mu}_s+\bar{\lambda}_s)F_2\beta+2\pi^2HR_{n2}^2\bar{H}^2F_2\\
&+4\pi^2HR_{n2}^2\bar{H}F_2\beta+2\pi^2HR_{n2}^2\beta^2F_2\\
&-4\pi^2HR_{n2}^2\beta\bar{H}-2\pi^2HR_{n2}^2\beta^2-2\pi^2HR_{n2}^2\bar{H}^2\\
&-2R_{n2}^2\pi^2\beta\bar{e}-2R_{n2}^2\pi^2\beta^2-\beta\bar{e}-\beta^2\\
&-2R_{n2}^2\pi^2(2\bar{\mu}_s+\bar{\lambda}_s)\bar{e}-2R_{n2}^2\pi^2(2\bar{\mu}_s+\bar{\lambda}_s)\beta\Big],
\end{aligned}
$$

$$
\begin{aligned}
k_{33}=&-\frac{\pi\beta F_1\upsilon}{12R_{n1}^3}\Big(6R_{n1}^4\pi^2\Delta x+6\pi^2\alpha^2\Delta xR_{n1}^2\\
&+\beta tn+2\pi^2\beta tnR_{n1}^2+R_{n1}^4\pi^4\beta tn+6\alpha^2\Delta\theta\\
&+6\Delta\theta R_{n1}^2+6\pi^2\alpha^2\Delta\theta R_{n1}^2+6R_{n1}^4\pi^4\Delta x\alpha^2\Big)\\
&-\frac{\pi F_1}{24R_{n1}^3}\Big[6R_{n1}^4\pi^4(2\bar{\mu}_s+\bar{\lambda}_s)R_{n1o}^2F_2\\
&-12R_{n1}^4\pi^2(2\bar{\mu}_s+\bar{\lambda}_s)\bar{\Delta}xF_2\\
&+6R_{n1}^4\pi^4(2\bar{\mu}_s+\bar{\lambda}_s)R_{n1I}^2F_2+12R_{n1}^4\pi^4(2\bar{\mu}_s\\
&+\bar{\lambda}_s)\bar{\Delta}x\alpha^2+12\pi^2\alpha^2(2\bar{\mu}_s+\bar{\lambda}_s)\bar{\Delta}xR_{n1}^2\\
&+12\pi^2\alpha^2(2\bar{\mu}_s+\bar{\lambda}_s)\bar{\Delta}\theta R_{n1}^2+4\pi^2\beta^2tnF_2R_{n1}^2\\
&+48\pi^2tn\alpha^2F_2R_{n1}^2+2R_{n1}^4\pi^4\beta^2tnF_2\\
&+24R_{n1}^4\pi^4tn\alpha^2F_2-12\pi^2C_{vdw}R_{n1o}\alpha^2R_{n1}^3\\
&+12\pi^2\alpha^2\Delta\theta\beta R_{n1}^2+12\pi^2\alpha^2\Delta x\beta R_{n1}^2\\
&+12R_{n1}R_{n1o}\alpha^2C_{vdw}F_2+12R_{n1}^4\pi^4\beta\Delta x\alpha^2\\
&+12R_{n1}^4\pi^2(2\bar{\mu}_s+\bar{\lambda}_s)\bar{\Delta}x-6R_{n1}^4\pi^4(2\bar{\mu}_s\\
&+\bar{\lambda}_s)R_{n1I}^2-6R_{n1}^4\pi^4(2\bar{\mu}_s+\bar{\lambda}_s)R_{n1o}^2\\
&+48R_{n1}^4\pi^2tnF_2-48\pi^2tn\alpha^2R_{n1}^2\\
&-24R_{n1}^4\pi^4tn\alpha^2-12R_{n1}R_{n1o}\alpha^2C_{vdw}\\
&+12C_{vdw}R_{n1o}F_2R_{n1}^3-12(2\bar{\mu}_s+\bar{\lambda}_s)\bar{\Delta}\theta F_2R_{n1}^2\\
&-12\alpha^2(2\bar{\mu}_s+\bar{\lambda}_s)\bar{\Delta}\theta F_2+12R_{n1}^4\pi^2\beta\Delta x\\
&+6\pi^2\rho\mathrm{VCF}^2v^2R_{n1I}^2R_{n1}^3\\
&+12\pi^2C_{vdw}R_{n1o}\alpha^2F_2R_{n1}^3\\
&-12R_{n1}^4\pi^4(2\bar{\mu}_s+\bar{\lambda}_s)\bar{\Delta}x\alpha^2F_2\\
&-12\pi^2\alpha^2(2\bar{\mu}_s+\bar{\lambda}_s)\bar{\Delta}xF_2R_{n1}^2\\
&-12(2\bar{\mu}_s+\bar{\lambda}_s)R_{n1}^2-48tnR_{n1}^2-24tn\alpha^2\\
&-12\beta R_{n1}^2-6(2\bar{\mu}_s+\bar{\lambda}_s)R_{n1I}^2-6(2\bar{\mu}_s\\
&+\bar{\lambda}_s)R_{n1o}^2+6\pi^4\rho\mathrm{VCF}^2v^2R_{n1I}^2\alpha^2R_{n1}^3\\
&-6\pi^2\rho\mathrm{VCF}^2v^2R_{n1I}^2F_2R_{n1}^3\\
&+6\pi^2\rho\mathrm{VCF}^2v^2R_{n1I}^2\alpha^2R_{n1}-R_{n1}^4\pi^4\beta^3\\
&+12\alpha^2\Delta\theta\beta+48tnF_2R_{n1}^2-12C_{vdw}R_{n1o}R_{n1}^3\\
&+12(2\bar{\mu}_s+\bar{\lambda}_s)F_2R_{n1}^2+12(2\bar{\mu}_s\\
&+\bar{\lambda}_s)\bar{\Delta}\theta R_{n1}^2+12\alpha^2(2\bar{\mu}_s\\
&+\bar{\lambda}_s)\bar{\Delta}\theta-48R_{n1}^4\pi^2tn+6(2\bar{\mu}_s\\
&+\bar{\lambda}_s)R_{n1o}^2F_2+6(2\bar{\mu}_s+\bar{\lambda}_s)R_{n1I}^2F_2\\
&+2\beta^2tnF_2+12\Delta\theta\beta R_{n1}^2-2\pi^2\beta^3R_{n1}^2\\
&+24tn\alpha^2F_2-\beta^3-6\pi^2\rho\mathrm{VCF}^2v^2R_{n1I}^2\alpha^2F_2R_{n1}\\
&-6\pi^4\rho\mathrm{VCF}^2v^2R_{n1I}^2\alpha^2F_2R_{n1}^3\Big],
\end{aligned}
$$

$$
\begin{aligned}
k_{34}=&\frac{\pi C_{vdw}R_{n1o}R_{n2}F_1}{2R_{n1}^3}\Big[-R_{n1}^2-\alpha^2-\pi^2\alpha^2R_{n1}^2\\
&+\pi^2\alpha^2F_2R_{n1}^2+F_2R_{n1}^2+\alpha^2F_2\Big],
\end{aligned}
$$

$$
\begin{aligned}
k_{43}=&\frac{\pi R_{n1}F_1}{4R_{n2}^4}\Big[2\alpha^2R_{n1o}C_{vdw}F_2R_{n2}\\
&-(2\bar{\mu}_s+\bar{\lambda}_s)R_{n1o}^2F_2-2R_{n1o}C_{vdw}R_{n2}^3\\
&-2\pi^2\alpha^2R_{n1o}C_{vdw}R_{n2}^3\\
&+2\pi^2\alpha^2R_{n1o}C_{vdw}F_2R_{n2}^3-(2\bar{\mu}_s+\bar{\lambda}_s)R_{n1I}^2F_2
\end{aligned}
$$

$$
\begin{aligned}
&- 2\alpha^2 R_{n1o} C_{vdw} R_{n2} + (2\bar{\mu}_s + \bar{\lambda}_s) R_{n1o}^2 \\
&+ (2\bar{\mu}_s + \bar{\lambda}_s) R_{n1I}^2 + 2R_{n1o} C_{vdw} F_2 R_{n2}^3 \Big], \\
k_{44} =& - \frac{\pi\beta F_1 \upsilon}{12 R_{n2}^3 R_{n1}^2} \Big[6\Delta\theta R_{n2}^2 R_{n1}^2 + R_{n2}^4 \pi^2 \beta tn \\
&+ 6R_{n2}^4 \pi^2 \Delta x R_{n1}^2 + 6\alpha^2 \Delta\theta R_{n1}^2 + \beta tn R_{n1}^2 \\
&+ 6\pi^2 \alpha^2 \Delta x R_{n1}^2 R_{n2}^2 + R_{n2}^4 \pi^4 \beta tn R_{n1}^2 \\
&+ \pi^2 \beta tn R_{n2}^2 R_{n1}^2 + 6R_{n2}^4 \pi^4 \alpha^2 \Delta x R_{n1}^2 \\
&+ 6\pi^2 \alpha^2 \Delta\theta R_{n1}^2 R_{n2}^2 \Big] \\
&- \frac{\pi F_1}{24 R_{n2}^4 R_{n1}^2} \Big[12 R_{n2}^5 \pi^2 \Delta x \beta R_{n1}^2 \\
&- 12\pi^2 R_{n2o} K_{nG} R_{n2}^4 R_{n1}^2 + 2R_{n2}^5 \pi^2 \beta^2 tn F_2 \\
&- 48\pi^2 tn\alpha^2 R_{n2}^3 R_{n1}^2 + 48\pi^2 tn F_2 R_{n2}^5 R_{n1}^2 \\
&- 12(2\bar{\mu}_s + \bar{\lambda}_s) \bar{\Delta}\theta F_2 R_{n2}^3 R_{n1}^2 \\
&+ 12\alpha^2 (2\bar{\mu}_s + \bar{\lambda}_s) \bar{\Delta}\theta F_2 R_{n2} R_{n1}^2 \\
&+ 12 R_{n2o} K_{nw} F_2 R_{n2}^4 R_{n1}^2 - 24 R_{n2}^5 \pi^4 \alpha^2 tn R_{n1}^2 \\
&+ 2\beta^2 tn F_2 R_{n2} R_{n1}^2 + 24\alpha^2 tn F_2 R_{n2} R_{n1}^2 \\
&+ 12\pi^2 (2\bar{\mu}_s + \bar{\lambda}_s) \bar{\Delta} x R_{n2}^5 R_{n1}^2 \\
&- 6\pi^4 (2\bar{\mu}_s + \bar{\lambda}_s) R_{n2}^5 R_{n1}^2 R_{n1I}^2 \\
&- 6\pi^4 (2\bar{\mu}_s + \bar{\lambda}_s) R_{n2}^5 R_{n1}^2 R_{n1o}^2 \\
&- 12\alpha^2 R_{n1o} C_{vdw} R_{n2}^2 R_{n1}^2 \\
&- 12\alpha^2 R_{n2o} K_{nw} R_{n2}^2 R_{n1}^2 + 12\alpha^2 \Delta\theta\beta R_{n2} R_{n1}^2 \\
&+ 12\alpha^2 R_{n2o} K_{nG} F_2 R_{n1}^2 + 12 R_{n2o} K_{nG} F_2 R_{n2}^2 R_{n1}^2 \\
&+ 12 R_{n1o} C_{vdw} F_2 R_{n2}^4 R_{n1}^2 - 2\pi^2 \beta^3 R_{n2}^3 R_{n1}^2 \\
&- \pi^4 \beta^3 R_{n2}^5 R_{n1}^2 - 24 tn\alpha^2 R_{n2} R_{n1}^2 \\
&+ 48 tn F_2 R_{n2}^3 R_{n1}^2 + 12(2\bar{\mu}_s + \bar{\lambda}_s) F_2 R_{n2}^3 R_{n1}^2 \\
&+ 12(2\bar{\mu}_s + \bar{\lambda}_s) \bar{\Delta}\theta R_{n2}^3 R_{n1}^2 \\
&- 12\alpha^2 R_{n2o} K_{nG} R_{n1}^2 - 12 R_{n2o} K_{nG} R_{n2}^2 R_{n1}^2 \\
&+ 12\Delta\theta\beta R_{n2}^3 R_{n1}^2 - 12 R_{n1o} C_{vdw} R_{n2}^4 R_{n1}^2 \\
&- 12 R_{n2o} K_{nw} R_{n2}^4 R_{n1}^2 - 48\pi^2 tn R_{n2}^5 R_{n1}^2 \\
&- 12(2\bar{\mu}_s + \bar{\lambda}_s) R_{n2}^3 R_{n1}^2 - 48 tn R_{n2}^3 R_{n1}^2 \\
&- \beta^3 R_{n2} R_{n1}^2 + 12\pi^2 \alpha^2 (2\bar{\mu}_s + \bar{\lambda}_s) \bar{\Delta} x R_{n2}^3 R_{n1}^2 \\
&+ 12\pi^2 \alpha^2 (2\bar{\mu}_s + \bar{\lambda}_s) \bar{\Delta}\theta R_{n2}^3 R_{n1}^2 \\
&- 12\pi^2 (2\bar{\mu}_s + \bar{\lambda}_s) \bar{\Delta} x F_2 R_{n2}^5 R_{n1}^2 \\
&+ 6R_{n1o}^2 \pi^4 (2\bar{\mu}_s + \bar{\lambda}_s) F_2 R_{n2}^5 R_{n1}^2 \\
&+ 6R_{n1I}^2 \pi^4 (2\bar{\mu}_s + \bar{\lambda}_s) F_2 R_{n2}^5 R_{n1}^2 \\
&+ 12\pi^4 \alpha^2 (2\bar{\mu}_s + \bar{\lambda}_s) \bar{\Delta} x R_{n2}^5 R_{n1}^2 \\
&+ 12\alpha^2 R_{n2o} K_{nw} F_2 R_{n2}^2 R_{n1}^2 \\
&+ 12\alpha^2 R_{n1o} C_{vdw} F_2 R_{n2}^2 R_{n1}^2 \\
&+ 12\pi^2 R_{n2o} K_{nG} F_2 R_{n2}^4 R_{n1}^2 \\
&+ 12\pi^4 \alpha^2 \Delta x \beta R_{n2}^5 R_{n1}^2 \\
&- 12\pi^2 R_{n1o} C_{vdw} \alpha^2 R_{n2}^4 R_{n1}^2 \\
&- 12\pi^4 \alpha^2 R_{n2o} K_{nG} R_{n2}^4 R_{n1}^2 \\
&- 12\pi^2 \alpha^2 R_{n2o} K_{nw} R_{n2}^4 R_{n1}^2 \\
&- 24\pi^2 \alpha^2 R_{n2o} K_{nG} R_{n2}^2 R_{n1}^2 \\
&+ 12\pi^2 \alpha^2 \Delta x \beta R_{n2}^3 R_{n1}^2 + 12\pi^2 \alpha^2 \Delta\theta\beta R_{n2}^3 R_{n1}^2 \\
&- 12\alpha^2 (2\bar{\mu}_s + \bar{\lambda}_s) \bar{\Delta}\theta F_2 R_{n2} R_{n1}^2 \\
&+ 2R_{n2}^5 \pi^4 \beta^2 tn F_2 R_{n1}^2 + 24 R_{n2}^5 \pi^4 \alpha^2 tn F_2 R_{n1}^2 \\
&+ 2\pi^2 \beta^2 tn F_2 R_{n2}^3 R_{n1}^2 + 48\pi^2 \alpha^2 tn F_2 R_{n2}^3 R_{n1}^2 \\
&- 12\beta R_{n2}^3 R_{n1}^2 + 12\pi^2 R_{n1o} C_{vdw} F_2 \alpha^2 R_{n2}^4 R_{n1}^2 \\
&+ 12\pi^2 \alpha^2 R_{n2o} K_{nw} F_2 R_{n2}^4 R_{n1}^2 \\
&+ 24\pi^2 \alpha^2 R_{n2o} K_{nG} F_2 R_{n2}^2 R_{n1}^2 \\
&- 12 R_{n2}^5 \pi^4 \alpha^2 (2\bar{\mu}_s + \bar{\lambda}_s) \bar{\Delta} x F_2 R_{n1}^2 \\
&- 12\pi^2 \alpha^2 (2\bar{\mu}_s + \bar{\lambda}_s) \bar{\Delta}\theta F_2 R_{n2}^3 R_{n1}^2 \\
&- 12\pi^2 \alpha^2 (2\bar{\mu}_s + \bar{\lambda}_s) \bar{\Delta} x F_2 R_{n2}^3 R_{n1}^2 \Big], \\
k_{55} =& \frac{1}{4} R_{n1} \pi^3 \beta \upsilon F_1 + \frac{\pi F_1}{4 R_{n1}} \Big[-2(2\bar{\mu}_s + \bar{\lambda}_s) \\
&- 2\beta - R_{n1}^2 \pi^2 \beta + 2(2\bar{\mu}_s + \bar{\lambda}_s) F_2 \Big],
\end{aligned}
$$

$$k_{66} = \frac{1}{4}R_{n2}\pi^3\beta\upsilon F_1 + \frac{\pi F_1}{4R_{n2}}\Big[-2(2\bar{\mu}_s + \bar{\lambda}_s) - 2\beta - R_{n2}^2\pi^2\beta + 2(2\bar{\mu}_s + \bar{\lambda}_s)F_2\Big],$$

$$KN_{33} = -\frac{K_1K_3}{R_{n1}^2}[W1^2R_{n1}^2 + 3W2^2R_{n2}^2],$$

$$KN_{34} = \frac{R_{n2}K_1K_3}{R_{n1}^3}[W_2^2R_{n2}^2 + 3W2^2R_{n1}^2],$$

$$KN_{43} = \frac{R_{n1}K_2K_3}{R_{n2}^3}[W1^2R_{n1}^2 + 3W2^2R_{n2}^2],$$

$$KN_{44} = -\frac{K_2K_3}{R_{n2}^2}[W2^2R_{n2}^2 + 3W1^2R_{n1}^2],$$

$$K_1 = \pi^2\alpha^2F_2R_{n1}^2 + F_2R_{n1}^2 - \alpha^2 - \pi^2\alpha^2R_{n1}^2 + \alpha^2F_2 - R_{n1}^2,$$

$$K_2 = \pi^2\alpha^2F_2R_{n2}^2 + F_2R_{n2}^2 - \alpha^2 - \pi^2\alpha^2R_{n2}^2 + \alpha^2F_2 - R_{n2}^2,$$

$$K_3 = \frac{9}{32}R_{n1o}C_NF_1\pi, \tag{A.1}$$

Biographies

Ali Ghorbanpour Arani received his BS degree from Sharif University of Technology, Tehran, Iran, in 1988, his MS degree from Amirkabir University of Technology, Tehran, Iran, in 1991, and his PhD degree from Esfahan University of Technology, Esfahan, Iran, in 2001. He is currently Professor in the Mechanical Engineering Faculty of the University of Kashan, Iran. He has authored more than 100 refereed journal papers and 9 books. His current research interests include stress analyses, stability and vibration of nanotubes, smart nanocompsites, and FGMs.

Mohammad Hashemian received his BS degree, in 2005, from the Islamic Azad University, Khomeinishahr, Iran, and his MS degree, in 2008, from the University of Kashan, Iran, where he is currently a PhD degree student. His research interests include nanomechanics, continuum mechanics, dynamic stability, buckling and vibration.